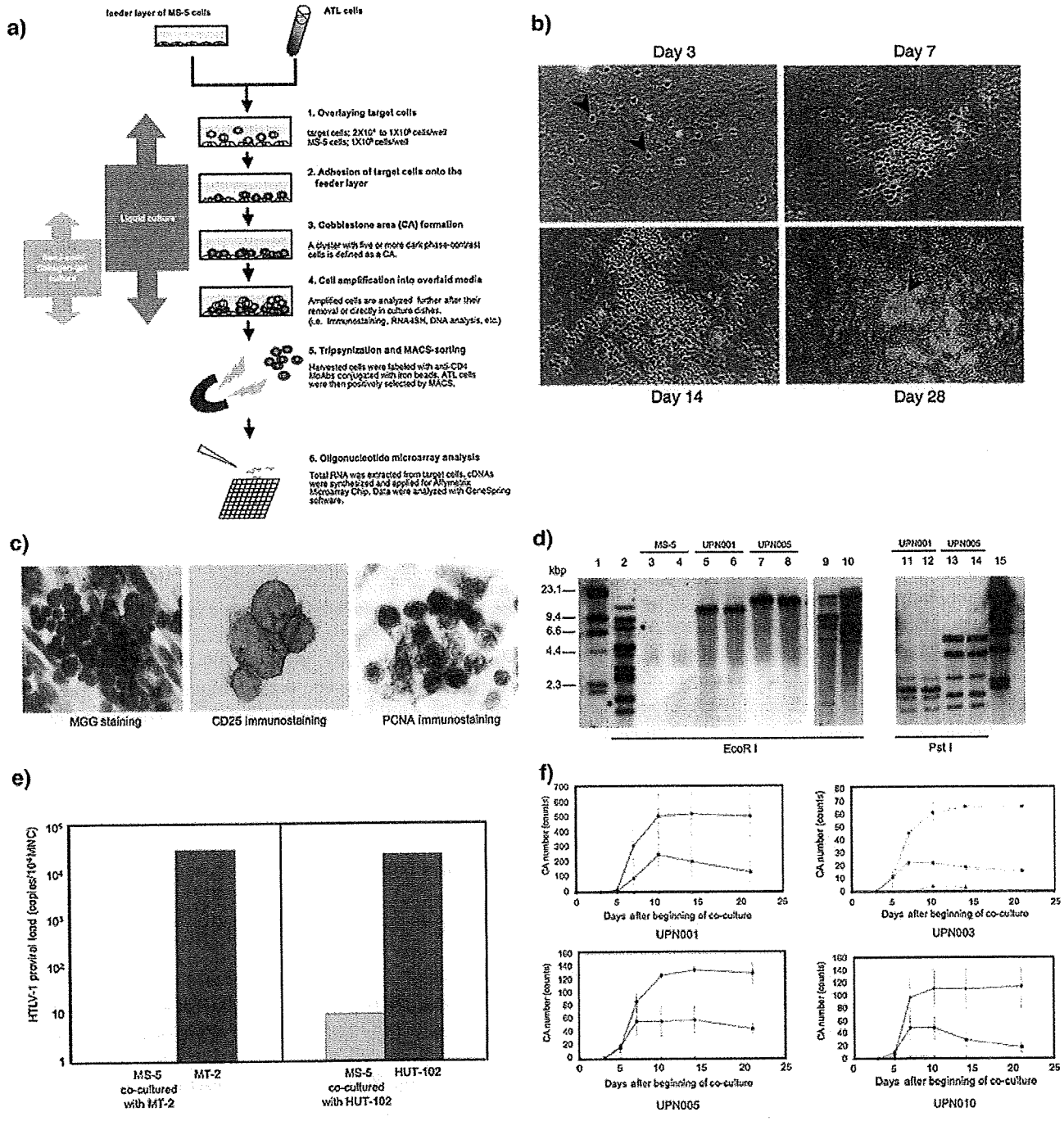

2.2 Monoclonal antibodies (MoAbs)

LT-4 (anti-p40Tax; mouse IgG_3) and Gin-7 (anti-p19Gag; mouse IgG2b) were used to detect Tax and Gag protein, respectively, by immunocytochemical staining [21, 22]. Leu3a (anti-CD4), Leu2a (anti-CD8), anti-Tac (anti-CD25), and PC-10 (anti-proliferating cell nuclear antigen (PCNA); DAKO Cytomation) were also used for immunophenotyping.

2.3 Co-culture system with a stromal layer of MS-5 cells

Murine marrow stromal MS-5 cells were kindly provided by Kirin Brewery Co. Ltd (Gunma, Japan). This cell line was originally established by Itoh et al. [17]. Maintenance of MS-5 cells and preparation of stromal feeder layers for co-culture experiments were as described previously [18]. The co-culture experiments are outlined in Fig. 1a. In short,

target cells were overlayed at various concentrations (2×10^4 to 1×10^5 cells/35 mm well) in RPMI1640 medium, including 20% fetal bovine serum (FBS), onto the feeder layer of MS-5 cells. The culture medium was changed twice a week. The culture dishes were observed daily under a phase-contrast microscope, and after an adequate period, cultured cells were processed in the following experiments.

In order to compare the capacity of target cell growth with the MS-5-stromal layer, co-culture experiments with HESS-5, which can support human hematopoietic cells in in vitro culture [23], or human umbilical venous endothelial cells (HUVEC) were performed. The murine marrow stroma cell line HESS-5 was kindly provided by the Pharmaceutical Frontier Research Laboratory, JT Inc. (Yokohama, Japan). HESS-5 cells were maintained in alpha-minimal essential medium (alpha-MEM; GIBCO) supplemented with 10% (v/v) horse serum (HS). HUVEC was purchased from Bio-Whittaker Inc., MD, USA, and maintained in accordance with the manufacturer's instructions.

In a few experiments, 2×10^5/mL ATL cells were cultured in RPMI1640 containing 20% FBS and 200 ng/mL recombinant human IL-2 (R&D systems) for five to seven days without any stromal feeder layers (liquid culture) for comparison studies with the co-culture system.

Strictly, to test the plating efficiency of primary ATL cells, we employed the Cellmatrix™ (Nitta gelatin Inc., Osaka, Japan) collagen gel culture kit according to the manufacturer's instructions. After verifying the formation of cellular clusters in a semi-solid state, these were counted under a phase-contrast microscope.

2.4 Immunocytostaining

Cells cultured on multi-chamber BioCoat/FALCON Culture Slides™ (Falcon Labware) were washed with phosphate-buffered saline (PBS). In some experiments, cytospin preparations were made from colony-composing cells and from liquid cultures. For immunostaining CD4, CD8, CD25, PCNA, and HTLV-1-related proteins, preparations were fixed with appropriate fixatives for each antigens, incubated with primary antibodies, and stained using the streptavidin–biotin-alkaline phosphatase-labeling method or the diaminobenzidine tetrahydrochloride-based horse-radish peroxidase reaction as described previously [24, 25]. To estimate the positive staining rate, a minimum of 200 ATL cells was observed under a light microscope with a final magnification of 1,000× (Nikon, Japan).

2.5 Southern blot hybridization (SBH) and HTLV-1 proviral load

The pattern of integration of the HTLV-1 provirus into the host genome was investigated using SBH as described previously [26]. In short, first, ATL cells, which proliferated in the co-culture system, were harvested by trypsinization. Cell suspension was collected from culture vessels, and subsequently left to settle for 30 min at 37°C in fresh flasks, which allowed for the separation of ATL cells from adherent MS-5 cells onto the bottom of the flasks. After harvesting the supernatant, which included many ATL cells, and MS-5 cells, separately, genomic DNA was extracted from them. Aliquots of DNA were digested with restriction enzyme of *Eco*RI or *Pst*I, and then processed for SBH using a digoxigenin-labeled whole HTLV-1.

HTLV-1 proviral load was quantified using a real-time DNA PCR LightCycler Technology System according to our previously described method [27]. The sample copy number was estimated by interpolation from the standard curve generated by serial dilution of a *tax*-containing plasmid.

2.6 Cell adhesion blockade analysis

To inhibit the adhesion of ATL cells to the MS-5 monolayer, a Cell Culture Insert™ membrane (Falcon) with 0.4 μm pore size, on which 5×10^4 target cells were overlayed in methylcellulose including 20%FBS/RPMI1640, was inserted into the 35 mm culture well with the MS-5 monolayer on the bottom of each dish. In some experiments of this setting, 20%FBS/RPMI1640 was substituted for conditioned medium (CM), which was harvested from co-culturing of MT-2 and MS-5 layer.

2.7 RNA in situ hybridization (ISH)

The mRNA expression of the HTLV-I *tax* gene was investigated by ISH using a synthetic single-stranded 40-base oligonucleotide probe corresponding to 7409-7453 of this genetic region. The sequences of the oligo-DNA probes were as follows [28]: antisense probe for *tax* mRNA: 3′-ACGCCCTACTGGCCACCTGTCCAGAGCATCAGA TCACCTG-5′, sense probe for *tax* mRNA: 3′-TGCG GGATGACCGGTGGACAGGTCTCGTAGTCTAGTGG AC-5′, and antisense probe for 28S ribosomal RNA as an internal control: 3′-TGCTACTACCACCAAGATCTGCA CCTGCGGCGGC-5′. These probes were conjugated with digoxigenin (DIG) at 3′. Unstained cytospin preparations and cultured chamber-slides were fixed for 10 min in 2% paraformaldehyde/PBS at room temperature. Subsequently, fixed preparations were processed using the Ventana HX Discovery™ (Ventana Medical Systems, Tucson, AZ) automated ISH instrument system according to the manufacturer's instructions. The conditions of each reaction were as follows: denaturation; for 10 min at 42 °C for 10 min, hybridization with oligo-probe; for 6 h at 37 °C, incubation with secondary antibody; for 30 min at 37 °C, and

colorization in streptavidin-conjugated HRP solution; for 90 min at 37 °C. The expression of the Tax gene was evaluated using a light microscope (Nikon, Japan) with a final magnification of 1,000×. A minimum of 200 ATL cells was observed in each specimen to estimate the positive staining rate. ATL cells were considered to have expressed the Tax gene when they displayed a blue–gray signal in their cytoplasm or nucleus.

2.8 Oligonucleotide microarray analysis

$CD4^+$ ATL cells were harvested from the co-culture system by trypsinization, and purified by MACS magnetic cell separation system (Miltenyi Biotec) immediately. Primary samples were also processed as described above, except for trypsinization. Enrichment of the $CD4^+$ fraction was evaluated by subjecting portions of MNC and $CD4^+$ cell preparations to analysis of the expression of CD4 by flow cytometry (FACSCaliber™; Becton-Dickinson, Mountain View, CA, USA). In all samples, the $CD4^+$ fraction constituted greater than 90% of the eluate of the affinity column. Total RNA was isolated from CD4-positive ATL cells using TRIzol reagent as described by the manufacturer (Life Technologies, Inc., Gaithersberg, MD), and then treated with RNase-free DNase I (RQ1 DNase) at 37 °C for 30 min (Promega, Madison, WI). The preparation of RNA and hybridization with HGU133A & B microarrays (Affymetrix, Santa Clara, CA, USA) were as described previously [29].

2.9 Quantification of mRNA levels using real-time PCR

Total RNA was used for cDNA synthesis using Oligo(dT)12–18 Primer (Invitrogen) and SuperScript TM3 Reverse Transcriptase (Invitrogen). Real-time PCR (*Taq*-Man) analysis was performed on a LightCycler (Roche) according to the manufacturer's instructions. Primers used for the validation studies of expression profiles are shown in Table 3. Experiments were performed with triplicates for each sample, and the glyceraldehydes-3 phosphate dehydrogenase (GAPDH) expression was used to normalize the expression of each gene for sample-to-sample differences in RNA input, RNA quality and reverse transcriptase efficiency. Furthermore, quantification of mRNA levels of HTLV-I basic leucine zipper factor (HBZ) and Tax genes was performed as described previously [30]. Assays were carried out in duplicate and the average value was used as absolute amounts of HBZ and Tax mRNA in samples.

2.10 Statistical analysis

The Mann–Whitney *U* test and Student's *t* test were used for statistical analysis with StatView software. To analyze the data of microarray analysis, the fluorescence intensity of each gene was normalized relative to the median fluorescence value for all human genes with a "Present" and "Marginal" call (Microarray Suite; Affymetrix) in each hybridization. Comparative analysis by fold change data was performed with GeneSpring 7.0 software (Silicon Genetics, Redwood, CA, USA).

3 Results

3.1 Growth of ATL cells in co-culture system with MS-5

HTLV-1-transformed and ATL patient-derived cell lines grew in close contact with the stromal layer of MS-5 cells and formed so-called "cobblestone areas" (CAs), which were made up of dark-contrasted clusters of growing cells under phase-contrast microscopy [31], without any exogenous cytokines. Not only IL-2-independent cell lines (MT-2, HUT-102, and OMT), but also two of three IL-2-dependent cell lines in our series, ST-1 and KOB, formed CAs without the addition of IL-2. KK-1 showed minimal growth in this culture system without IL-2.

Next, ATL cells from clinical samples were also used in this co-culture system. In representative cases, which showed prosperous growth, ATL cells adhered and crept into the stromal layer in a few days from the start of co-culture, grew with formation of CAs from day 10 to 14, and continued to grow over three weeks and proliferated upward into the medium out of CA cells in the third or fourth week of co-culture (Fig. 1b). In eight of 10 (80.0%) samples of acute ATL and one sample of lymphoma type, CA formation was observed, whereas three samples from two patients with chronic type of ATL, one with smoldering type and the control peripheral T cells obtained from healthy volunteers with Con-A stimulation did not have CA-forming cells (Table 1).

In May-Grunwald-Giemsa (MGG) staining, growing cells in CAs showed small lymphocyte-type morphology with convoluted nuclei as primary ATL cells show, although some growing cells showed immature, namely blastic features, which differed from primary malignant cells in the peripheral blood obtained from the patients. Immunostaining of CD4 and CD8 revealed that these cells had the immunophenotype of helper T cells, which were identical to primary ATL cells. Furthermore, since PCNA immunostaining in CA-composing cells from ATL showed a positive reaction, these cells were assumed to be in a growth phase (Fig. 1c). In two cases (UPN001 and 005), SBH analysis revealed that the integration pattern of the HTLV-1 provirus in ATL cells composing CA in each case was identical to that in primary ATL cells (Fig. 1d).

Table 1 Proliferation assay of primary ATL cells co-cultured with MS-5 cells

UPN	Subtype	Material	Frequency of clonogenic cells (%)		
			CAFC	Colony formation	
				IL-2 (+)[a]	IL-2 (−)
001	Acute	PE	1.04	0	0
		PB	0.78	0	0
002	Acute	PB	0	0	0
003	Acute	LN	0.32	0	0
004	Acute	PB	0.03	0	0
		LN	0.05	0	0
005	Acute	PB	0.12	0	0
006	Acute	PB	0.08	0	0
007	Acute	PB	0.25	0	0
008	Acute	LN	0.31	0	0
009	Acute	PB	0	0	0
010	Acute	LN	0.25	0	0
011	Lymphoma	LN	0.68	0	0
012	Chronic	PB	0	0.034	0
013	Chronic	PB	0	0.012	0
014	Chronic	PB	0.014	0.031	0
015	Smoldering	PB	0	0	0
016	Healthy[b]	PB	0	nd	nd
017	Healthy[b]	PB	0.008	nd	nd

PB peripheral blood, *LN* lymph node, *PE* pleural effusion

[a] Concentration of IL-2 was 200 ng/ml

[b] Con-A-stimulated (10 ng/ml) T cells were cultured

Table 2 Inhibitory effect of contact between ATL cells and stromal layer of MS-5

Sample	Frequency of clonogenic cells (%)						
	CAFC		Colony formation				
MS-5 stroma	+	+	+	+	+	−	−
Contact inhibition[a]	−	−	+	+	+	−	−
Co-cultured CM[b]	−	−	−	+	−	+	−
Exogenous IL-2[c]	−	+	−	−	+	−	+
UPN005 (acute)	0.12	0.21	0	0	0	0	0
UPN006 (acute)	0.08	0.06	0	0	0	0	0
UPN007 (acute)	0.25	0.24	0	0	0	0	0
UPN009 (chronic)	0	0.08	0	0.08	0	0	0.08

[a] A CellCulture Insert™ membrane was inserted to the co-culture system to inhibit direct cell–cell interaction between ATL cells and MS-5 cell layer. Values represent frequency of CAFC or colony-forming unit in the co-culture system and in the co-culture system with contact inhibition or in conditions without a MS-5 layer, respectively

[b] In this condition, we added conditioned medium (CM) which was harvested from co-culturing of MT-2 and MS-5 layer

[c] Concentration of IL-2 was 200 ng/ml

3.2 Significance of adhesion of ATL cells to stromal layer

A contact-inhibition experiment with a Cell Culture Insert™ membrane inserted in culture dishes was performed for four cases (three cases of acute type and one case of chronic type). In all three acute cases, CAs formed only under conditions, which allowed for close contact with the stromal layer of MS-5 cells. There was no colony formation in methylcellulose semi-solid cultures under contact inhibition to the stromal layer using Cell Culture Insert™, or without a stromal layer, regardless of stimulation by exogenous IL-2 or co-cultured CM. In a chronic subtype, although there was no CA formation in this co-culture system, colony formation was observed with IL-2 stimulation (Table 2). SBH analysis and quantification studies of HTLV-1 viral load revealed that infection of HTLV-1 to MS-5 cells was not detected in co-culturing with MT-2, although slightly detected in co-culturing with HUT-102 (Fig. 1d, e).

Compared with the MS-5 stromal layer, significantly less CA formed in co-culture with the HESS-5 stromal layer after day 7 of co-culturing, although we could observe comparable adhesion and growth of target cells on both stromal layers at earlier phase. Furthermore, there was no sustainable CA formation in co-culture with HUVEC (Fig. 1f). We applied the co-culture system with the MS-5 stromal layer in further analysis because of its superior efficiency for CA formation.

The semi-solid collagen gel culture of five primary ATL samples [UPN001 (PB), 003, 005, 007, and 011] revealed a linear relationship between the inoculated cell number and CA count, indicating that this assay system would be useful to quantify clonogenic precursors of ATL cells, i.e., CA-forming cells (CAFC) (Fig. 2a; Table 1). In our series, the frequency of CAFC in acute or lymphoma type varied considerably, ranging from 0.03 to 1.04% (median 0.25), and was significantly higher than in chronic type or healthy donors ($P < 0.01$; Fig. 2b).

3.3 HTLV-1 proviral gene expression in neoplastic CAs

The production of Tax and Gag proteins in ATL cells co-cultured with a stromal layer were examined by immunostaining and ISH. Based on immunostaining, these proteins seemed to disappear in CAs in ATL cell lines, HUT-102 and ST-1 (Fig. 3a).

Four cases of acute-type ATL showed a strong staining pattern for these proteins in primary neoplastic cells after liquid culture with stimulation by IL-2; however, ATL cells in CA showed significantly weaker staining for Tax and Gag proteins in all four cases (Fig. 3b). Furthermore, in

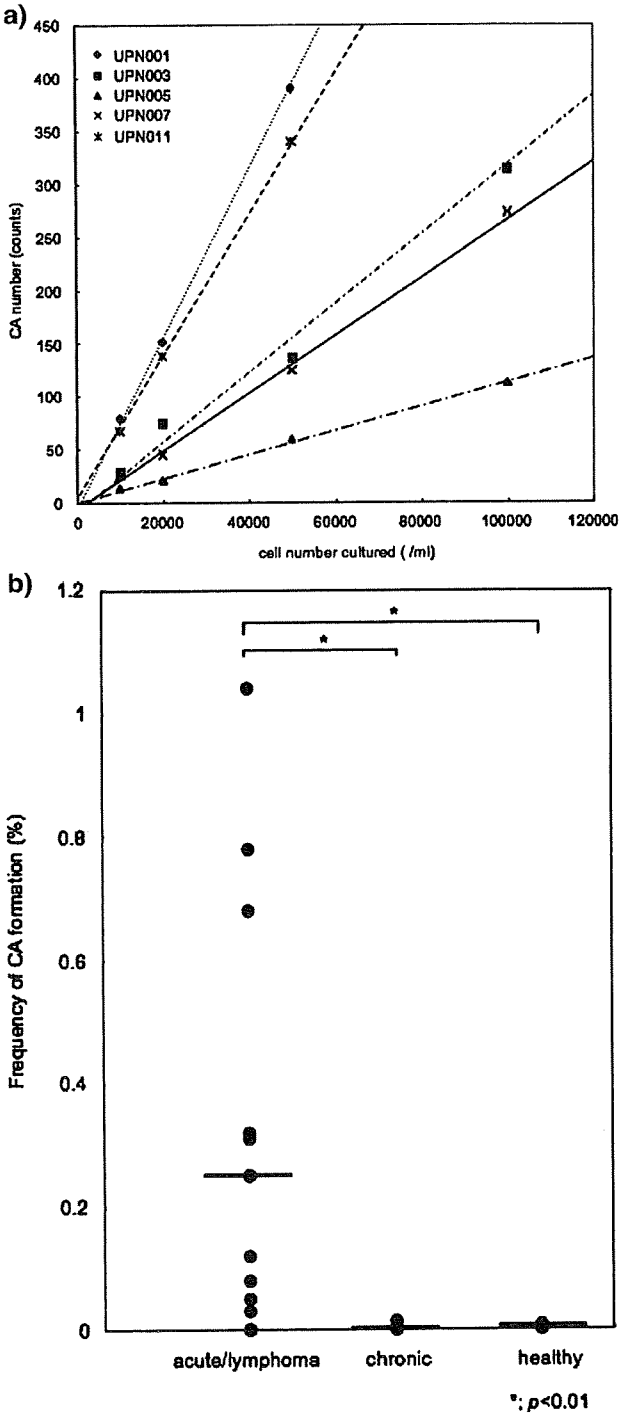

Fig. 2 Plating efficiency of ATL cells in a co-culture system with MS-5 cells. **a** The frequency of CA-forming cells (CAFC) of five cases (UPN001 (PB), 003, 005, 007, and 011) was examined with semi-solid collagen gel in the co-culture system. A clear linear relationship was obtained between the inoculated cell number and CAFCs in all cases examined. **b** The distribution plots of frequency of CA formation in different sample group; There is statistical difference in the median (*horizontal bars*) among acute/lymphoma type (0.25%), chronic type (0%), and healthy volunteers (0.04%) ($P < 0.01$)

three cases of acute ATL, the results of ISH revealed that the expression of the Tax gene of ATL cells in CA was markedly decreased when compared with that of growing cells in liquid culture with IL-2 (Fig. 3c).

Next, we quantified the expression level of HBZ gene, which was recently identified in the 3″-LTR of the complementary sequence of HTLV-1 and has been suggested as a critical gene in leukemogenesis of ATL [6, 32, 33]. As shown in Fig. 3d, the HBZ gene was highly expressed in MT-2 cells in CA, and the level of mRNA load was equivalent to those without co-culturing. With regard to *tax* gene, the expression level was significantly higher in cells in liquid culture without stroma than in cells in CA, although the difference was not so striking as observed in RNA-ISH analysis. Moreover, in the contact-inhibited condition to the stromal layer, the expression levels of these two genes were comparable to those without co-culturing.

3.4 Gene expression profiles of ATL cells composing CA

Next, we compared the gene expression profiles of sets of ATL cells composing CA matched with their corresponding $CD4^+$ primary samples from the same individuals by high-density oligonucleotide microarray analysis, to search for candidates of disease-specific molecules and signaling pathways, which contribute to the mechanism of adhesion-dependent proliferation in our co-culture system. After removal of transcriptionally silent genes from the analysis of 44,764 probe sets using Microarray Suite software, Student's *t* test ($P < 0.001$) was then used to extract genes, the expression level of which significantly differed between cells in CA and primary samples. Genes were considered up- or down-regulated if each value and the average fold change were 3.5 or greater in all three data sets. Finally, we could identify 110 and 98 genes significantly up- and down-regulated in ATL cells in CA compared with primary samples by selecting genes based on the reproducibility, respectively (Fig. 4a).

To validate the microarray findings, we performed RTQ-PCR for eight genes that were significantly up- or down-regulated in ATL cells in CA of three-paired array samples, and with code products correlating with adhesion molecules and cell–cell interaction or with cellular apoptosis and proliferation. All experiments were performed in triplicate. Variance among triplicates was less than 5%. Standard curves with correlation coefficiency greater than 0.970 were produced from the data for each gene, indicating the large dynamic range and accuracy of RTQ-PCR (data not shown). As shown in Table 3 and Fig. 4b, we confirmed that these genes were actually up- or down-regulated in ATL cells in CA, compared with primary

neoplastic cells as indicated in the microarray data. Up-regulated genes, *CDH11* [34], *Twist1* [35] and *Cav-1* [36], are considered to play a major role in tumor promotion, progression, survival and metastasis in several neoplasias. Furthermore, the down-regulation of several genes, *hCdc14A* [37], *CUGBP2* [38], *HBP1* [39], and *ZNFN1A1* [40], the products of which are recognized to play a role in suppressing carcinogenesis through various signaling pathways, were also confirmed in ATL cells in CA.

4 Discussion

In the present study, we established a new ATL cell/murine stroma cell co-culture system with which we could observe the proliferation of primary ATL cells without any additional growth factor. In previous studies, primary ATL cells were able to grow in a liquid culture containing IL-2; however, they showed only a transient and cytokine-dependent proliferation [8–10]. On the other hand, we also observed involvement of HTLV-1 genome to patients' LN stroma cells and production of several cytokines from them [16]. In the present study, infection of HTLV-1 to MS-5 was considered to be dispensable to adhesion-dependent ATL cell growth, as shown in the negative or minimal viral load in co-cultured MS-5 cells. Furthermore, since many murine cytokines cannot affect human cells [41], and especially in this co-culture system, any soluble factor or co-cultured CM did not stimulate ATL cells growth in the contact-inhibition test, direct adhesion of target cells to the stromal layer of MS-5 layers are considered to be essential for CA formation by primary ATL cells in this co-culture system.

In the lymphohematopoietic microenvironment, normal and neoplastic lymphoid cells are affected by various molecules [42, 43]. Concerning lymphoid malignancies, recent reports has indicated that interactions between neoplastic cells and BM or LN stromal cells regulate growth, survival, and homing in multiple myeloma, mantle cell lymphoma, and other non-Hodgkin lymphoma [44, 45]. Whereas, the expression of various adhesion molecules and chemokine receptors on leukemic cells, also in ATL, is assumed to be essential to the pathophysiology of this disease [46–50], the significance of these molecules in the growth and survival of ATL cells is still poorly understood. Thus, extensive investigation of the molecular interaction between neoplastic cells and lymphohematopoietic microenvironment is essential to clarify not only adhesion and transmigration, but also the growth and survival mechanism of primary ATL cells in this co-culture system.

In the present study, two murine stromal cell lines, MS-5 and HESS-5 showed significant supportive capacity on leukemic CA formation comparing with HUVEC, and also indicated their differential abilities for support of growth and survival of target cells. Both of them were originally established from C3H/HeN strain mice and might share common characters concerning the interaction between hematopoietic cells and stroma layer through integrin family members [51, 52]. Furthermore, target cells could adhere and start to grow on both stromal layers in our series. Our limited studies did not reveal the mechanism of differential abilities to support the growth of ATL cells between MS-5 and HESS-5 with respect to the direct interaction to target cells for the maintenance of CA formation. Previous reports concerning successful xeno-transplantation of ATL cells into immunodeficient mice indicated that indispensable extrinsic elements might be supplied to human neoplastic cells in these in vivo animal models sharing similarity with human lymphohematopoietic microenvironment [53, 54]. In analogy, our in vitro

Fig. 3 Expression of HTLV-1-related genes in ATL cells in CA. ▶ **a** HUT-102 and ST-1 cells were examined by phase-contrast micrographs (final magnification ×400), May-Giemsa staining (final magnification ×600), and immunostaining of Tax protein on ATL cells in CA and on cells after liquid culture using anti p40Tax antibody, Lt-4 (final magnification ×400). **b** Expression of HTLV-1 viral proteins on ATL cells in CA obtained from primary ATL cells. Four patients with acute-type ATL were examined. *Color* photographs show representative results of immunostaining of Tax (*upper*) and Gag (*lower*) in primary cells after culture with IL-2 for 7 days (*left*) and ATL cells in CA (*right*) (UPN004). *Bar graphs* are a summary of results of immunostaining of Tax and Gag protein in four cases. Light and *dark gray bars* indicate the results of primary ATL cells after liquid culture with IL-2 and those of ATL cells in CA in our co-culture system, respectively. Data are presented as the mean percentage of positive cells in triplicate experiments with error bars indicating 1SD. Mann–Whitney's *U* test was performed for statistical analysis and, in every sample, the positive rate of immunostaining of p19 and p40 was significantly lower in ATL cells in CA than in primary ATL cells after liquid culture with IL-2 ($P < 0.01$). **c** *tax* mRNA expression in ATL cells in CA obtained from primary ATL cells. ATL cells obtained from three cases were analyzed by RNA-ISH method. *Color* photographs show representative results of the analysis of UPN001; primary ATL cells after liquid culture with IL-2 (*left*) and ATL cells in CA (*right*): tested with the probe to 28S ribosomal RNA as an internal control (*upper*), the antisense oligonucleotide probe to the *tax* mRNA (*middle*), and the sense oligonucleotide probe (*lower*), indicated in "Sect. 2". Areas surrounded by arrowheads are CAs. *Bar graphs* are a summary of the results of three primary samples, which were analyzed RNA-ISH for *tax* mRNA. Light and dark gray bars indicate the results of primary ATL cells after liquid culture with IL-2 and those of ATL cells in CA in our co-culture system, respectively. Data are presented as the mean percentage of positive cells in triplicate experiments with error bars indicating 1SD. Mann–Whitney's *U* test was performed for statistical analysis and, in every sample, the positive rate of *tax* mRNA expression was significantly lower in ATL cells in CA than in primary ATL cells after liquid culture with IL-2 ($P < 0.01$). **d** Results of quantification of mRNA load of HBZ and *tax* genes. The copy number of target mRNA per 50 ng total RNA was estimated from the standard curves [29]. *Light* and *dark gray* and *white bars* indicate data, which were obtained from HUT-102 and MT-2 cell lines in three different culture conditions; conventional liquid culture, co-culture with MS-5, and contact-inhibited condition to MS-5 stromal layer, respectively

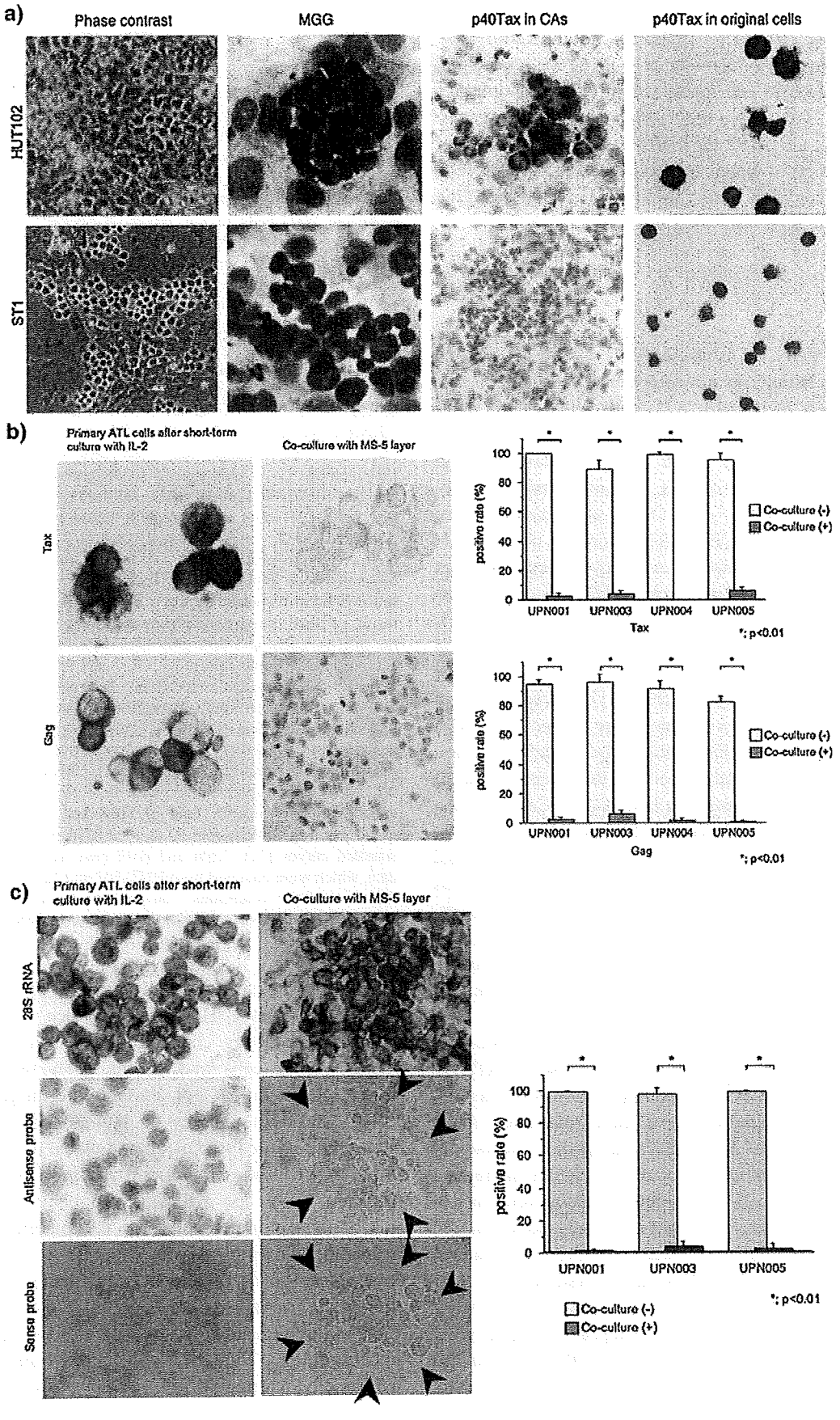
a)
Phase contrast
MGG
p40Tax in CAs
p40Tax in original cells
HUT102
ST1
b)
Primary ATL cells after short-term culture with IL-2
Co-culture with MS-5 layer
Tax
Gag
positive rate (%)
Co-culture (-)
Co-culture (+)
UPN001
UPN003
UPN004
UPN005
*; p<0.01
c)
Primary ATL cells after short-term culture with IL-2
Co-culture with MS-5 layer
28S rRNA
Antisense probe
Sense probe

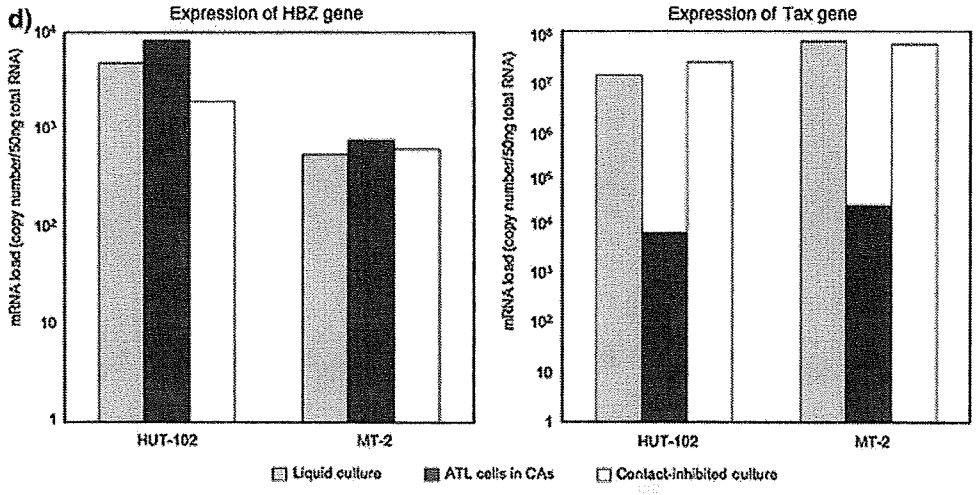

Fig. 3 continued

co-culture system is also considered to provide ATL cells with common factors with in vivo adhesion-dependent growth mechanism of ATL cells.

Although neoplastic cells of lymphoid malignancies have been considered to proliferate primarily in lymphoid tissues, there are so far few cell lines established from LN stroma and available for reproducible analysis of neoplastic cell growth. Since ATL cells frequently invade and proliferate in BM, especially in aggressive phase, this co-culture system is considered to provide components which are necessary for growth and survival of neoplastic cells in BM microenvironment. Surprisingly, we reported previously that in a semi-solid colony assay system, IL-2-dependent colony formation occurred in almost all cases of chronic or smoldering type, but rarely in acute and lymphoma types [55]. These results observed among our limited number of clinical cases indicate that in the prodromal phase of ATL, some cytokines were needed for the growth of neoplastic cells in vitro, while in a more aggressive phase, such a cytokine-dependency declines and some aberrant signal transducers might contribute to a more autonomous proliferation and enhance survival of ATL cells through anti-apoptotic process, which is considered to be closely related to stroma-dependent cell growth.

It has been demonstrated recently in several cancers, especially leukemias, that neoplastic cells are heterogeneous in terms of their capacity to grow and self renew, and that only a small proportion of cells are actually clonogenic in culture and also in vivo [56]. Many recent evidences indicate that microenvironment contributes significantly to tumorigenesis originated from such "cancer stem cells" [57]. In the present study, the leukemic CAFCs exhibited clonogenic potential by showing a linear relationship between inoculated ATL cells and CA numbers as carefully enumerated in the semi-solid collagen gel culture. Furthermore, in four of eight acute-type cases, which gave rise to primary growth, we could observe the secondary CA formation in replating experiments (data not shown). Although it remains controversial whether there exists such a hierarchy in a malignant clone of ATL, our observation supports the hypothesis that there might be a neoplastic stem cell system also in ATL, and future studies on the cellular biology of leukemic CAFCs would shed light on our knowledge of this concept, especially in the context of interaction with the microenvironment of lymphohematopoietic tissue. This is important in that any treatment modality must eradicate such clonogenic cells that are quiescent or proliferating in close contact with stromal cells to obtain a cure.

In the present study, immunostaining and RNA-ISH analysis revealed that our co-culture system allowed the growth of primary ATL cells even with a trace amount of Tax, at the level of transcription and translation. On the other hand, expression of HBZ gene in ATL cells was not affected by our co-culture system. Interestingly, this difference in expression pattern of two genes apparently resembles the behavior of ATL cells in vivo. Together with the result of mRNA load assay in the adhesion blockade system and the finding of reappearance of Tax protein in ATL cell lines which grew upward from the CAs and detached from the MS-5 monolayer into the culture medium (data not shown), it is suggested that there might be a direct interaction between ATL cells and stromal layer as a regulatory mechanism of *tax* gene expression, including epigenetic modification, in this co-culture system. Furthermore, we believe that further investigation of the actions of the *HBZ* gene in this unique in vitro culture system is important to clarify not only regulatory mechanism of *tax* gene expression [58], but also interactions between microenvironment and ATL

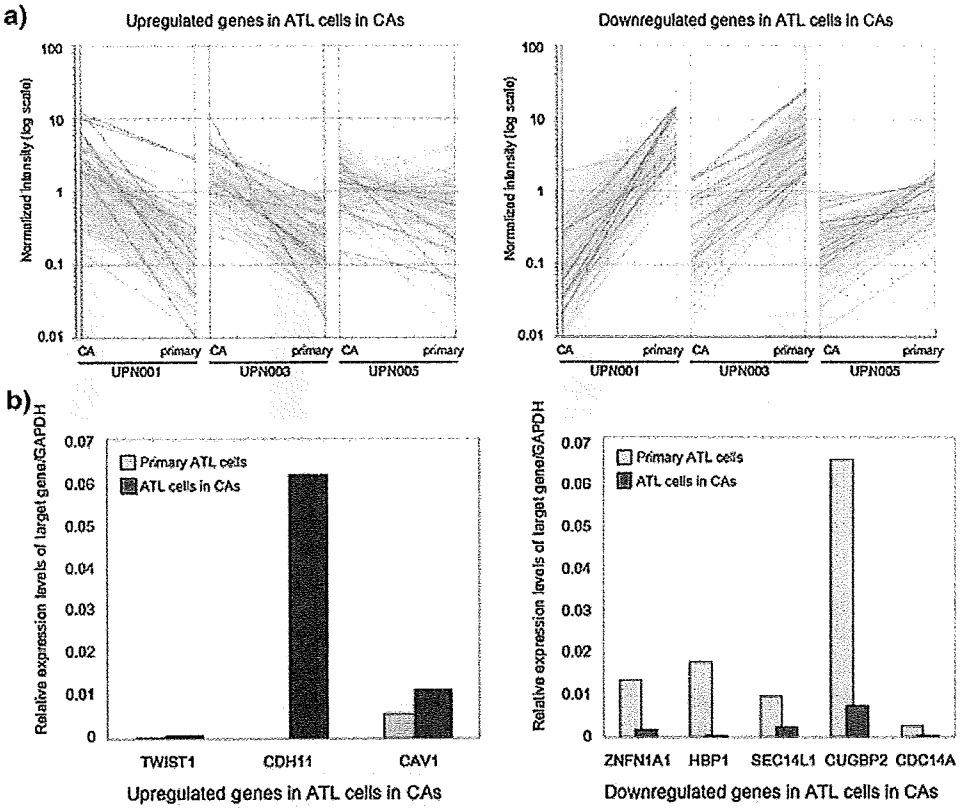

Fig. 4 Comparative studies of gene expression profiles between ATL cells in CA and corresponding primary cells from three clinical samples. For the expression data set of subjects, we first set a condition in which the expression level of a given gene should receive the "Present" call [from Microarray Suite 5.0 (Affymetrix)] in at least 60% (four samples) of the samples, aiming to remove transcriptionally silent genes from the analysis. The mean expression intensity of the internal positive control probe sets (http://www.affymetrix.com/support/technical/mask_files.affx) was set to 500U in each hybridization, and the fluorescence intensity of each test gene was normalized accordingly. **a** Diagrams of comparative profiles of three matched ATL cells in CA and their corresponding $CD4^+$ primary samples from the same individuals (UPN001, UPN003, and UPN005); up-regulated genes (*left*) and down-regulated genes (*right*) in ATL cells in CA. **b** Validation of the expression of eight selected genes from the expression profiles by RTQ-PCR. Primers and probes used in this study are shown in Table 3. Results are expressed in *graphs* of primary cells (*light gray bars*) and those of ATL cells in CA (*dark gray bars*) as fold differences between samples in their target gene expression relative to their levels of GAPDH. Standard curves were generated for each gene with tenfold serial dilution (100×10^{-6}) of cDNA from the KOB cell line and lymphocytes obtained from healthy volunteers. After confirming the precise log-linear relation of the standard curve, the final results were expressed as fold differences between samples in their target gene expression relative to their levels of GAPDH

cells for their growth and survival. This co-culture system is considered to be useful for the analysis of ATL cell growth and survival in a condition without excessive effect of Tax which was always present in the former in vitro culture systems.

Application of transcriptional profiling of ATL cells in CA revealed that there were no significant difference between ATL cells composing CA and primary ATL cells in expression level of several molecules, which play important roles in signaling pathways in ATL, including NFkB pathway. NFkB and related molecules have been shown to be constitutively activated in vivo without expression of Tax [59], although the mechanism of the constitutive activation of NFkB is still unclear. Therefore, several essential signaling pathways could also contribute to the growth of ATL cells under the adhesion-dependent and Tax-independent condition, which apparently resembles in vivo proliferation. On the other hand, interestingly also, we confirmed significant up- and down-regulation of several adhesion molecules and adaptor proteins, which play important roles in signaling pathways through cell-cell or cell-matrix interaction in ATL cells in CA. Taken together, these findings are assumed to indicate that our co-culture system might expose novel molecular mechanisms, which specifically regulate the growth and survival of clonogenic ATL cells. We believe that "outside-in" signaling pathways from interaction with the microenvironment might control such a mechanism in ATL cells. Further investigations are needed to elucidate the precise functions of these molecules.

Recently, a number of novel therapeutic agents to treat neoplastic diseases have been developed, as the growth

Table 3 Genes whose expressions were up- or down-regulated in ATL cells in CA compared with corresponding primary cells as determined by microarray analysis and validated by RTQ-PCR

Gene title	Genbank Accession ID	Description	Primers	Product size	Fold change
Upregulated genes in CAs					
CDH11	D21254	Osteoblast-cadherin	S CTGGAACCATTTTTGTGATT AS TCCACCGAAAAATAGGGTTG	343 bp	32.93
TWIST1	X99268	Twist-related protein 1, H-Twist, Twist homolog 1 (acrocephalosyndactyly 3; Saethre-Chotzen syndrome)	S GTCCGCAGTCTTACGAGGAG AS CCAGCTTGAGGGTCTGAATC	159 bp	5.026
CAV1	AU147399	Caveolin 1, caveolae protein	S CGCACACCAAGGAGATCGA AS GTGTCCCTTCTGGTTCTGCAAT	106 bp	5.301
Downregulated genes in CAs					
CDC14A	NM_003672	CDC14 cell division cycle 14 homolog A	S GCACTTACAATCTCACCATTC AS CATGTTGTAATCCCTTTCTG	58 bp	0.0748
CUGBP2	N36839	CUG triplet repeat, RNA binding protein 2	S CCTTTGAGGACTGCCATTGT AS TGAGGGGGAAAGTCCTTTTT	236 bp	0.0723
SEC14L1	AI017770	SEC14 like 1 protein	S TCCAAGAGGTCGCCACAACCAC AS AGAGACCTGCAGGGACGCAA	288 bp	0.0686
HBP1	AI689935	High mobility group (HMG) box transcription factor 1	S GCTTCCTTTGCAATGGTTCT AS CTGTGCAGCTCACATCTGTATG	243 bp	0.0646
ZNFN1A1	NM_018563	DNA-binding protein Ikaros, Zinc finger protein, subfamily 1A, 1	S CGAGTTCTCGTCGCACATAA AS ATCAAACCCCAATCAACCAA	221 bp	0.0571

Matching primers and fluorescence probes were designed for each of the genes selected by microarray data, employing PRIMER3 software (http://www.genome.wi.mit.edu/cgi-bin/primer/primer3_www.cgi) using sequence data from the NCBI database

mechanism of neoplastic cells becomes clearer at the molecular level. We have previously reported that this co-culture system could be used to test the sensitivity of neoplastic progenitors of Philadelphia chromosome (Ph^1)/BCR-ABL-positive leukemia to p210 tyrosine kinase inhibitor, imatinib mesylate (Gleevec^{TM}) [18]. This observation provides evidence that our co-culture system is extremely valuable for testing human tumor cells to grow using similar signaling pathways as in vivo. IL-2-dependent T cell lines established from a bulk liquid culture were usually clonally different from primary ATL cells [60], whereas our co-culture system exhibited growth of primary ATL cells which were identical clone to clinical samples as shown in SBH analysis, indicating the superiority of our method for the study of primary ATL cells as a surrogate assay system to predict response of neoplastic progenitors to therapeutic candidate drugs.

5 Conclusion

The present study showed that our newly established ATL cell/murine stroma cell co-culture system is highly efficient for the assay of primary ATL cell growth. Further investigation should focus on the elucidation of novel disease-specific signaling pathways starting from adhesion molecules and extracellular matrix proteins in this co-culture system, which contribute to adhesion-dependent proliferation and survival of ATL cells with a resemblance of expression pattern of proviral genes to that of in vivo ATL cells. This achievement might also be useful in developing novel therapeutic agents targeting ATL progenitors.

Acknowledgments The present study was supported by grants-in-aid from the Ministry of Education, Science and Culture of Japan (12670992) and by the twenty-first Century Center of Excellence (COE) Program of Nagasaki University "International Consortium for Medical Care of Hibakusha and Radiation Life Science".

References

1. Uchiyama T, Yodoi J, Sagawa K, Takatsuki K, Uchino H. Adult T cell leukemia: clinical and hematologic features of 16 cases. Blood. 1977;50:481–92.
2. Takatsuki K. Adult T-cell leukemia. Intern Med. 1995;34:947–52.
3. Yoshida M, Miyoshi I, Hinuma Y. Isolation and characterization of retrovirus from cell lines of human adult T-cell leukemia and its implication in the disease. Proc Natl Acad Sci USA. 1982;79:2031–5.
4. Yoshida M, Seiki M, Yamaguchi K, Takatsuki K. Monoclonal integration of human T-cell leukemia provirus in all primary tumors of adult T-cell leukemia suggests causative role of human

T-cell leukemia virus in the disease. Proc Natl Acad Sci USA. 1984;81:2534–7.
5. Arisawa K, Soda M, Endo S, Kurokawa K, Katamine S, Shimokawa I, et al. Evaluation of adult T-cell leukemia/lymphoma incidence and its impact on non-Hodgkin lymphoma incidence in southwestern Japan. Int J Cancer. 2000;85:319–24.
6. Yasunaga J, Matsuoka M. Leukaemogenic mechanism of human T-cell leukaemia virus type I. Rev Med Virol. 2007;17:301–11.
7. Aboud M, Golde DW, Bersch N, Rosenblatt JD, Chen IS. A colony assay for in vitro transformation by human T cell leukemia virus type 1 and type 2. Blood. 1987;70:432–6.
8. Uchiyama T, Hori T, Tsudo M, Wano Y, Umadome H, Tamori S, et al. Interleukin-2 receptor (Tac antigen) expressed on adult T cell leukemia cells. J Clin Invest. 1985;76:446–53.
9. Lunardi-Iskandar Y, Gessain A, Lam VH, Gallo RC. Abnormal in vitro proliferation and differentiation of T-cell colony forming cells in patients with tropical spastic paraparesis/human T lymphocyte virus type 1 (HTLV-1) associated myeloencephalopathy and healthy HTLV-1 carrier. J Exp Med. 1993;177:741–50.
10. Seiki M, Hattori S, Hirayama Y, Yoshida M. Human adult T-cell leukemia virus: complete nucleotide sequence of provirus genome integrated in leukemia cell DNA. Proc Natl Acad Sci USA. 1983;80:3618–22.
11. Yoshida M. Multiple viral strategies of HTLV-1 for dysregulation of cell growth control. Annu Rev Immunol. 2001;19:475–96.
12. Basbous J, Gaudray G, Devaux C, Mesnard JM. Role of the human T-cell leukemia virus type I Tax protein in cell proliferation. Recent Res Dev Mol Cell Biol. 2002;3:155–66.
13. Peloponese JM Jr, Kinjo T, Jeang KT. Human T-cell leukemia virus type 1 Tax and cellular transformation. Int J Hematol. 2007;86:101–6.
14. Kinoshita T, Shimoyama M, Tobinai K, Ito M, Ito S, Ikeda S, et al. Detection of mRNA for the tax1/rex1 gene of human T-cell leukemia virus type-1 in fresh peripheral blood mononuclear cells of adult T-cell leukemia patients and viral carriers by using the polymerase chain reaction. Proc Natl Acad Sci USA. 1989; 86:5620–4.
15. Ohshima K, Hashimoto K, Izumo S, Suzumiya J, Kikuchi M. Detection of human T lymphotropic virus type 1 (HTLV-1) DNA and mRNA in individual cells by polymerase chain reaction (PCR) in situ hybridization (ISH) and reverse transcription (RT)-PCR ISH. Hematol Oncol. 1996;14:91–100.
16. Joh T, Yamada Y, Seto M, Kamihira S, Tomonaga M. High establishment efficiency of lymph node stromal cells which spontaneously produce multiple cytokines derived from adult T-cell leukemia/lymphoma patients. Int J Oncol. 1996;9:619–24.
17. Itoh K, Tezuka H, Sakoda H, Konno M, Nagata K, Uchiyama T, et al. Reproducible establishment of hemopoietic supportive stromal cell lines from murine bone marrow. Exp Hematol. 1989;17:145–53.
18. Kawaguchi Y, Jinnai I, Nagai K, Yagasaki F, Yakata Y, Matsuo T, et al. Effect of a selective Abl tyrosine kinase inhibitor, STI571, on in vitro growth of BCR–ABL-positive acute lymphoblastic leukemia cells. Leukemia. 2001;15:590–4.
19. Maeda T, Yamada Y, Moriuchi R, Sugahara K, Tsuruda K, Joh T, et al. Fas gene mutation in the progression of adult T cell leukemia. J Exp Med. 1999;189:1063–71.
20. Shimoyama M, Members of the Lymphoma Study Group. Diagnostic criteria and classification of clinical subtypes of adult T-cell leukemia-lymphoma. A report from the Lymphoma Study Group. Br J Haematol (1984–1987) 1991;79:428–37.
21. Tanaka Y, Masuda M, Yoshida A, Shida H, Nyunoya H, Shimotohno K, et al. An antigenic structure of the trans-activator protein encoded by human T-cell leukemia virus type-1 (HTLV-1), as defined by a panel of monoclonal antibodies. AIDS Res Hum Retroviruses. 1992;8:227–35.
22. Tanaka Y, Lee B, Inoi T, Tozawa H, Yamamoto N, Hinuma Y. Antigens related to three core proteins of HTLV-I (p24, p19 and p15) and their intracellular localizations, as defined by monoclonal antibodies. Int J Cancer. 1986;37:35–42.
23. Tsuji T, Ogasawara H, Aoki Y, Tsurumaki Y, Kodama H. Characterization of murine stromal cell clones established from bone marrow and spleen. Leukemia. 1996;10:803–12.
24. Nagai K, Sohda H, Kuriyama K, Kamihira S, Tomonaga M. Usefulness of immunocytochemistry for phenotypical analysis of acute leukemia; improved fixation procedure and comparative study with flow cytometry. Leuk Lyphoma. 1995;16:319–27.
25. Adams JC. Heavy metal intensification of DAB-based HRP reaction products. J Histochem Cytochem. 1981;29:775.
26. Tsukasaki K, Ikeda S, Murata K, Maeda T, Atogami S, Sohda H, et al. Characteristics of chemotherapy-induced clinical remission in long survivors with aggressive adult T-cell leukemia/lymphoma. Leuk Res. 1993;17:157–66.
27. Kamihira S, Dateki N, Sugahara K, Hayashi T, Harasawa H, Minami S, et al. Significance of HTLV-1 proviral load quantification by real-time PCR as a surrogate marker for HTLV-1-infected cell count. Clin Lab Haematol. 2003;25:111–7.
28. Miyazato A, Kawakami K, Iwakura Y, Saito A. Chemokine synthesis and cellular inflammatory changes in lung of mice bearing p40tax of human T-lymphotropic virus type 1. Clin Exp Immunol. 2000;120:113–24.
29. Choi YL, Tsukasaki K, O'Neill MC, Yamada Y, Onimaru Y, Matsumoto K, et al. A genomic analysis of adult T-cell leukemia. Oncogene. 2007;26:1245–55.
30. Usui T, Yanagihara K, Tsukasaki K, Murata K, Hasegawa H, Yamada Y, et al. Characteristic expression of HTLV-1 basic zipper factor (HBZ) transcripts in HTLV-1 provirus-positive cells. Retrovirology. 2008;5:34–44.
31. Breems DA, Blokland EA, Neben S, Ploemacher RE. Frequency analysis of human primitive hematopoietic stem cell subsets using a cobblestone area forming cell assay. Leukemia. 1994;8:1095–104.
32. Satou Y, Yasunaga J, Yoshida M, Matsuoka M. HTLV-I basic leucine zipper factor gene mRNA supports proliferation of adult T cell leukemia cells. Proc Natl Acad Sci USA. 2006;103:720–5.
33. Mesnard JM, Barbeau B, Devaux C. HBZ, a new important player in the mystery of adult T-cell leukemia. Blood. 2006;108:3979–82.
34. Tomita K, van Bokhoven A, van Leenders GJ, Ruijter ET, Jansen CF, Bussemakers MJ, et al. Cadherin switching in human prostate cancer progression. Cancer Res. 2000;60:3650–4.
35. Alexander NR, Tran NL, Rekapally H, Summers CE, Glackin C, Heimark RL. *N-cadherin* Gene Expression in Prostate Carcinoma Is Modulated by Integrin-Dependent Nuclear Translocation of Twist1. Cancer Res. 2006;66:3365–9.
36. Williams TM, Lisanti MP. Caveolin-1 in oncogenic transformation, cancer, and metastasis. Am J Physiol Cell Physiol. 2005;288:494–506.
37. Paulsen MT, Starks AM, Derheimer FA, Hanasoge S, Li L, Dixon JE, et al. The p53-targeting human phosphatase hCdc14A interacts with the Cdk1/cyclin B complex and is differentially expressed in human cancers. Mol Cancer. 2006;5:25.
38. Mukhopadhyay D, Houchen CW, Kennedy S, Dieckgraefe BK, Anant S. Coupled mRNA Stabilization and Translational Silencing of Cyclooxygenase-2 by a Novel RNA Binding Protein, CUGBP2. Mol Cell. 2003;11:113–26.
39. Zhang X, Kim J, Ruthazer R, McDevitt MA, Wazer DE, Paulson KE, et al. The HBP1 transcriptional repressor participates in RAS-induced premature senescence. Mol Cellular Biol. 2006; 26:8252–66.

40. Rebollo A, Schmitt C. Ikaros, Aiolos and Helios: transcription regulators and lymphoid malignancies. Immunol Cell Biol. 2003;81:171–5.
41. Issaad C, Croisille L, Katz A, Vainchenker W, Coulombel M. A murine stromal cell line allows the proliferation of very primitive human CD34^{++}/CD38- progenitor cells in long-term cultures and semisolid assays. Blood. 1993;81:2916–24.
42. Bajénoff M, Egen JG, Koo LY, Laugier JP, Brau F, Glaichenhaus N, et al. Stromal cell networks regulate lymphocyte entry, migration, and territoriality in lymph nodes. Immunity. 2006; 25:989–1001.
43. Woolf E, Grigorova I, Sagiv A, Grabovsky V, Feigelson SW, Shulman Z, et al. Lymph node chemokines promote sustained T lymphocyte motility without triggering stable integrin adhesiveness in the absence of shear forces. Nat Immunol. 2007;8:1076–85.
44. Mitsiades CS, McMillin DW, Klippel S, Hideshima T, Chauhan D, Richardson PG, et al. The role of the bone marrow microenvironment in the pathophysiology of myeloma and its significance in the development of more effective therapies. Hematol Oncol Clin North Am. 2007;21:1007–34.
45. Lwin T, Hazlehurst LA, Dessureault S, Lai R, Bai W, Sotomayor E, et al. Cell adhesion induces p27Kip1-associated cell-cycle arrest through down-regulation of the SCFSkp2 ubiquitin ligase pathway in mantle-cell and other non-Hodgkin B-cell lymphomas. Blood. 2007;110:1631–8.
46. Tanaka Y, Kimata K, Wake A, Mine S, Morimoto I, Yamakawa N, et al. Heparan sulfate proteoglycan on leukemic cells is primarily involved in integrin triggering and its mediated adhesion to endothelial cells. J Exp Med. 1996;184:1987–97.
47. Imura A, Hori T, Imada K, Kawamata S, Tanaka Y, Imamura S, et al. OX40 expressed on fresh leukemic cells from adult T-cell leukemia patients mediates cell adhesion to vascular endothelial cells: implications for the possible involvement of OX40 in leukemic cell infiltration. Blood. 1997;89:2951–8.
48. Hiraiwa N, Hiraiwa M, Kannagi R. Human T-cell leukemia virus-1 encoded Tax protein transactivates alpha 1 → 3 fucosyltransferase Fuc-T VII, which synthesizes sialyl Lewis X, a selectin ligand expressed on adult T-cell leukemia cells. Biochem Biophys Res Commun. 1997;231:183–6.
49. Tanaka Y, Minami Y, Mine S, Hirano H, Hu CD, Fujimoto H, et al. H-Ras signals to cytoskeletal machinery in induction of integrin-mediated adhesion of T cells. J Immunol. 1999;163: 6209–16.
50. Sasaki H, Nishikata I, Shiraga T, Akamatsu E, Fukami T, Hidaka T, et al. Overexpression of a cell adhesion molecule, TSLC1, as a possible molecular marker for acute-type adult T-cell leukemia. Blood. 2005;105:1204–13.
51. Suzuki J, Fujita J, Taniguchi S, Sugimoto K, Mori KJ. Characterization of murine hematopoietic-supportive (MS-1 and MS-5) and non-supportive (MS-K) cell lines. Leukemia. 1992;6:452–8.
52. Tsuji T, Waga I, Tezuka K, Kamada M, Yatsunami K, Kodama H. Integrin beta2 (CD18)-mediated cell proliferation of HEL cells on a hematopoietic-supportive bone marrow stromal cell line, HESS-5 cells. Blood. 1998;91:1263–71.
53. Dewan MZ, Terashima K, Taruishi M, Hasegawa H, Ito M, Tanaka Y, et al. Rapid tumor formation of human T-cell leukemia virus type 1-infected cell lines in novel NOD-SCID/gammac(null) mice: suppression by an inhibitor against NF-kappaB. J Virol. 2003;77:5286–94.
54. Imada K, Takaori-Kondo A, Akagi T, Shimotohno K, Sugamura K, Hattori T, et al. Tumorigenicity of human T-cell leukemia virus type I-infected cell lines in severe combined immunodeficient mice and characterization of the cells proliferating in vivo. Blood. 1995;86:2350–7.
55. Hata T, Fujimoto T, Tsushima H, Murata K, Tsukasaki K, Atogami S, et al. Multi-clonal expansion of unique human T-lymphotropic virus type-1-infected T cells with high growth potential in response to interleukin-2 in prodromal phase of adult T cell leukemia. Leukemia. 1999;13:215–21.
56. Reya T, Morrison SJ, Clarke MF, Weissman IL. Stem cells, cancer, and cancer stem cells. Nature. 2001;414:105–11.
57. Bissell MJ, LaBarge MA. Context, tissue plasticity, and cancer: Are tumor stem cells also regulated by the microenvironment? Cancer Cell. 2005;7:17–23.
58. Gaudray G, Gachon F, Basbous J, Biard-Piechaczyk M, Devaux C, Mesnard JM. The complementary strand of the human T-cell leukemia virus type 1 RNA genome encodes a bZIP transcription factor that down-regulates viral transcription. J Virol. 2002; 76:12813–22.
59. Mori N, Fujii M, Ikeda S, Yamada Y, Tomonaga M, Ballard DW, et al. Constitutive activation of NF-kappaB in primary adult T-cell leukemia cells. Blood. 1999;93:2360–8.
60. Yamada Y, Nagata Y, Kamihira S, Tagawa M, Ichimaru M, Tomonaga M, et al. IL-2-dependent ATL cell lines with phenotypes differing from the original leukemia cells. Leukemia Res. 1991;15:619–25.

Oncogene (2008) 27, 3102–3110
 0950-9232/08 $30.00
www.nature.com/onc

ORIGINAL ARTICLE

The FLT3 inhibitor PKC412 exerts differential cell cycle effects on leukemic cells depending on the presence of FLT3 mutations

T Odgerel[1], J Kikuchi[1], T Wada[1], R Shimizu[1], K Futaki[1], Y Kano[2] and Y Furukawa[1]

[1]*Division of Stem Cell Regulation, Center for Molecular Medicine, Jichi Medical School, Tochigi, Japan and* [2]*Division of Hematology, Tochigi Cancer Center, Tochigi, Japan*

PKC412 is a staurosporine derivative that inhibits several protein kinases including FLT3, and is highly anticipated as a novel therapeutic agent for acute myeloblastic leukemia (AML) carrying FLT3 mutations. In this study, we show that PKC412 exerts differential cell cycle effects on AML cells depending on the presence of FLT3 mutations. PKC412 elicits massive apoptosis without markedly affecting cell cycle patterns in AML cell lines with FLT3 mutations (MV4-11 and MOLM13), whereas it induces G_2 arrest but not apoptosis in AML cell lines without FLT3 mutations (THP-1 and U937). In MV4-11 and MOLM13 cells, PKC412 inactivates Myt-1 and activates CDC25c, leading to the activation of CDC2. Activated CDC2 phosphorylates Bad at serine-128 and facilitates its translocation to the mitochondria, where Bad triggers apoptosis. In contrast, PKC412 inactivates CDC2 by inducing serine-216 phosphorylation and subsequent cytoplasmic sequestration of CDC25c in THP-1 and U937 cells. As a result, cells are arrested in the G_2 phase of the cell cycle, but do not undergo apoptosis because Bad is not activated. The FLT3 mutation-dependent differential cell cycle effect of PKC412 is considered an important factor when PKC412 is combined with cell cycle-specific anticancer drugs in the treatment of cancer and leukemia.
Oncogene (2008) **27**, 3102–3110; doi:10.1038/sj.onc.1210980; published online 10 December 2007

Keywords: FLT3 inhibitor; leukemia; cell cycle; CDC2; CDC25; Bad

Introduction

FMS-like tyrosine kinase-3 (FLT3) is a member of class III receptor tyrosine kinases, and is expressed on hematopoietic stem/progenitor cells. The binding of FLT3 ligand induces dimerization and autophosphorylation of FLT3, and subsequently activates multiple signal transduction pathways favoring cell survival and proliferation (Lyman *et al.*, 1993; Small *et al.*, 1994). FLT3 is also expressed in the majority of acute leukemias and is overexpressed in many cases (Gilliland and Griffin, 2002). In addition, its mutations are found in approximately 30% of patients with acute myeloblastic leukemia (AML), and accordingly, these are the second most common genetic alterations in AML. FLT3 mutations include internal tandem duplication of the juxtamembrane domain (FLT3-ITD) and point mutations in the activating loop, both of which result in ligand-independent activation of FLT3. The constitutive activation of FLT3 appears to promote aberrant proliferation and survival of hematopoietic stem/progenitor cells, leading to leukemogenesis (Kelly *et al.*, 2002).

Because of the high frequency of mutations and overexpression, FLT3 should be an appropriate therapeutic target in AML (Griffin, 2004). It has been shown that the staurosporine derivative PKC412 inhibits multi-target tyrosine kinases, including FLT3, protein kinase C, CDC2 and receptors for PDGF, FGF and VEGF (Levis and Small, 2005). PKC412 induces apoptosis in blasts from AML patients with FLT3 mutations, and prolongs survival in animal models of FLT3-induced myeloproliferative diseases (Weisberg *et al.*, 2002). Clinical trials for patients with solid tumors and AML revealed that PKC412 alone yielded limited clinical activity (Propper *et al.*, 2001; Stone *et al.*, 2005). To overcome this limitation, it is reasonable to combine PKC412 with other conventional antileukemic agents.

Recently, we have reported that PKC412 has synergistic effects with most antileukemic agents for FLT3-mutated leukemia cell lines (Furukawa *et al.*, 2007). In contrast, PKC412 is antagonistic to most drugs, except for those inducing mitotic arrest or active in the G_2/M phase in leukemia cell lines without FLT3 mutations. This finding provides useful information for the design of effective combination therapy containing PKC412. For safe and effective clinical applications, however, it is essential to clarify the molecular basis of the FLT3 mutation-dependent divergence of leukemic cell responses to PKC412. In this study, we attempted to resolve this issue by analysing the effects of PKC412 on the expression of cell cycle regulators and Bcl-2 family proteins in AML cell lines with or without FLT3 mutations.

Correspondence: Professor Y Furukawa, Division of Stem Cell Regulation, Center for Molecular Medicine, Jichi Medical School, 3311-1 Yakushiji, Shimotsuke, Tochigi 329-0498, Japan.
E-mail: furuyu@jichi.ac.jp
Received 2 July 2007; revised 5 November 2007; accepted 6 November 2007; published online 10 December 2007

Results

Effects of PKC412 on growth kinetics of AML cell lines with or without FLT3 mutations

We first compared the sensitivity to PKC412 of four AML cell lines: MOLM13, MV4-11, THP-1 and U937. It has been shown that MOLM13 and MV4-11 cell lines carry FLT3-ITD (internal tandem duplication), whereas FLT3 is in wild-type configuration in THP-1 and U937 cell lines (Quentmeier *et al.*, 2003). THP-1 cells express a large amount of FLT3 but U937 cells do not express FLT3 (Yao *et al.*, 2003). In pilot experiments, we determined the dose–response curves at day 3 (data not shown), and calculated the IC_{50} values for MOLM13, MV4-11, THP-1 and U937 to be 38 ± 4, 34 ± 6, 116 ± 26 and 207 ± 41 nM, respectively. On the basis of this result, we treated these cell lines with 100 nM PKC412 and observed the changes in growth kinetics. As shown in Figure 1a, PKC412 almost completely inhibited an increase in cell numbers of MOLM13 and MV4-11 cell lines. Growth inhibition was accompanied by the abrogation of constitutive phosphorylation of FLT3 (Figure 1b). The effects of PKC412 on other possible targets were variable and not correlated with cytotoxicity (Figure 1c and Supplementary Figure 1), suggesting that FLT3 is a principal target of PKC412-mediated growth inhibition of MOLM13 and MV4-11 cells. The proliferation of THP-1 cells was also markedly suppressed by PKC412, whereas U937 cells were relatively resistant to the drug (Figure 1a, lower panel). It is of note that the steady-state growth of AML cell lines with FLT3 mutations (MOLM13 and MV4-11) was significantly slower than that of AML cell lines without FLT3 mutations (THP-1 and U937) (Figure 1a, upper panel).

Cell cycle analysis of PKC412-treated AML cell lines

Next, we attempted to clarify the underlying mechanisms of PKC412-mediated growth inhibition of AML cell lines using cell cycle analysis. PKC412-induced apoptosis, as judged by an increase in the size of the sub-G_1 fraction (see Figure 2a for representative results, and Table 1 for quantification and statistical analysis of three independent experiments), DNA fragmentation (Figure 2b) and the appearance of apoptotic bodies (Figure 2c), in MOLM13 and MV4-11 cell lines after 24 h of culture without markedly affecting cell cycle distribution except for a minor decrease in the fraction of cells in the growth phases (S and G_2/M phases). In contrast, THP-1 and U937 cells were arrested in the G_2 phase by PKC412 after 12 h of treatment, and underwent mitotic slippage to become hyperploid after 48 h, especially in the latter (Figure 2 and Table 1). Apoptosis was barely observed in these cell lines up to 48 h of culture.

The difference of the changes in cell cycle distribution between PKC412-treated AML cell lines with FLT3-ITD and those with wild-type FLT3 may provoke the differential responses of cells to the combination of PKC412 and cell cycle-modifying drugs. To verify this

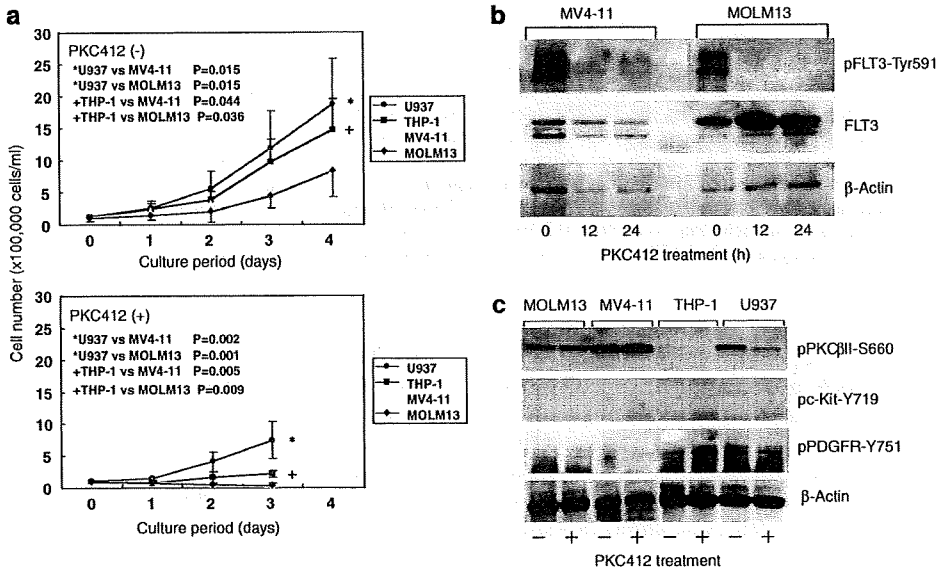

Figure 1 Effects of PKC412 on cell growth and FLT3 phosphorylation of acute myeloblastic leukemia (AML) cell lines. (**a**) We seeded AML cell lines at an initial concentration of 1×10^5 cells ml^{-1}, and cultured in the absence (upper panel) or presence (lower panel) of 100 nM PKC412 for up to 4 days. Viable cells were counted after staining with erythrosine B dye. The means ± s.d. (bars) of three independent experiments are shown. Statistical analysis was performed using Student's *t*-test. (**b**) Whole cell lysates were prepared from MV4-11 and MOLM13 cells cultured with 100 nM PKC412 at the indicted time points, and subjected to immunoblotting with an antibody that specifically recognizes FLT3 phosphorylated at tyrosine-591 (pFLT3-Tyr591). The membranes were reblotted with anti-FLT3 and β-actin antibodies to serve as loading controls. (**c**) Whole cell lysates were prepared from four cell lines before (–) and after (+) culture with 100 nM PKC412 for 24 h, and used for the detection of the indicated proteins. Data shown are representative of multiple independent experiments.

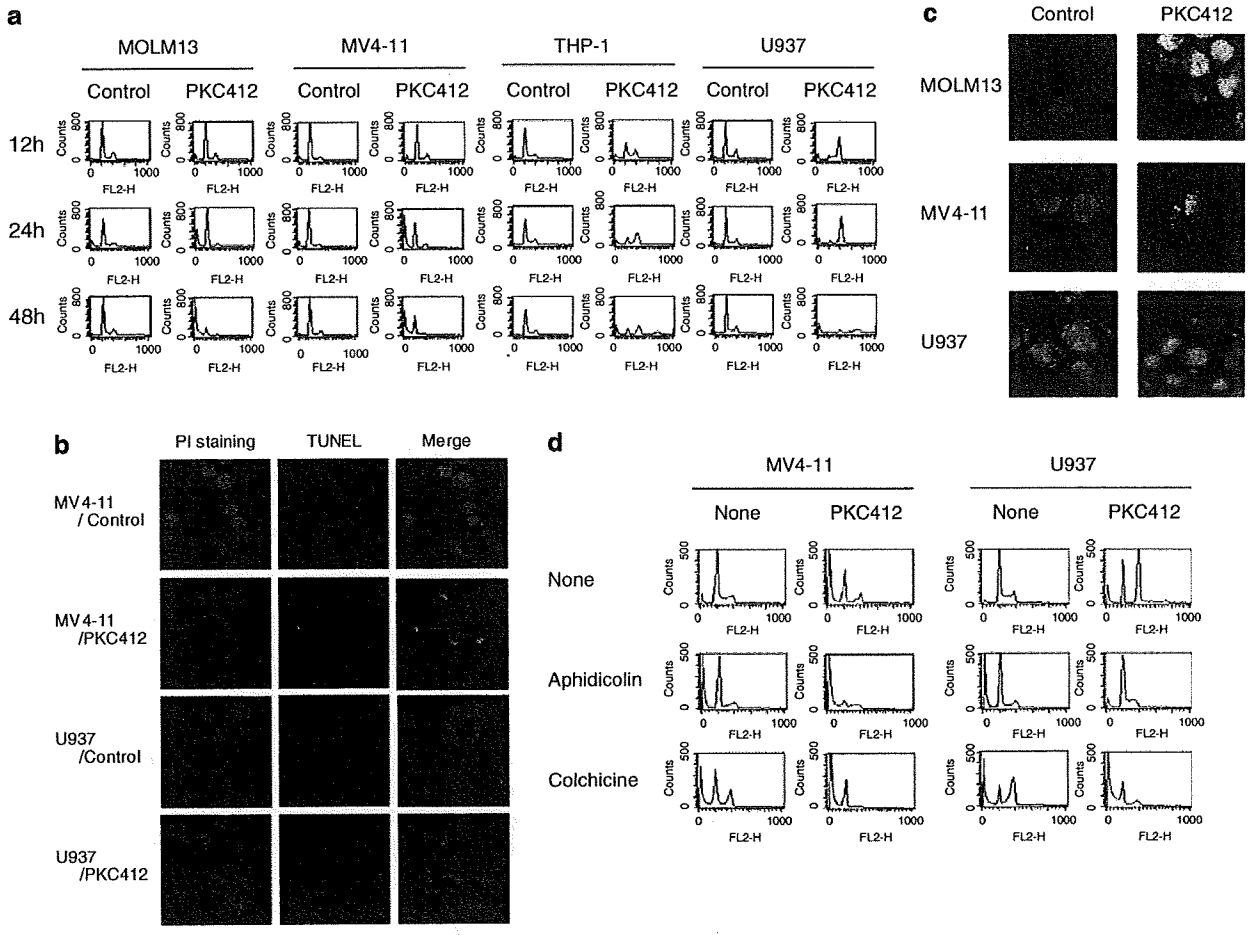

Figure 2 Differential effects of PKC412 on the cell cycle of acute myeloblastic leukemia (AML) cell lines with or without FLT3 mutations. MOLM13, MV4-11, THP-1 and U937 cells were seeded at 1×10^5 cells ml^{-1}, and cultured in the absence (control) or presence (PKC412) of 100 nM PKC412. (**a**) Cells were harvested at the indicated time points, and stained with propidium iodide in preparation for cell cycle analysis. See Table 1 for quantification and statistical analysis. (**b**) After 24 h of culture, cells were harvested for the detection of DNA fragmentation by the TUNEL method. Fragmented DNA was labeled with biotin-dUTP and stained with avidin-conjugated fluorescein isothiocyanate (FITC; TUNEL). Intact DNA was counterstained with propidium iodide (PI staining). Original magnification is ×400 for all panels. (**c**) After 24 h of culture, cells were stained with an antitubulin antibody (green fluorescence) and propidium iodide (red fluorescence). Original magnification is ×600 for all panels. (**d**) MV4-11 and U937 cells were cultured with (aphidicolin and colchicine) or without (none) cell cycle-modifying drugs in the absence (none) or presence (PKC412) of PKC412. The concentrations of each drug were PKC412 100 nM, aphidicolin 1 mg ml^{-1} and colchicine 100 nM. After 24 h of culture, cells were harvested for cell cycle analysis. The data shown are representative of three independent experiments.

hypothesis, we examined the combined effects of PKC412 and either aphidicolin, which induces G_1/S arrest by inhibiting DNA polymerase α, or colchicine, which arrests cells at mitosis by disrupting mitotic spindle. As shown in Figure 2d, PKC412 was synergistic with both aphidicolin and colchicine in MV4-11 cells, but only with colchicine in U937 cells. This is fully consistent with the pattern of cell cycle changes induced by PKC412 in each cell line.

PKC412 differentially modulates the phosphorylation of CDC2 in AML cell lines depending on the presence of FLT3 mutations

The above results indicate that PKC412 inhibits the growth of AML cells via distinct mechanisms depending on the presence of FLT3 mutations. We investigated the underlying mechanisms of differential responses to PKC412. First, we checked the phosphorylation status of CDC2, which reflects its activity *in vivo*, in PKC412-treated AML cell lines. As shown in Figure 3a, CDC2 was heavily phosphorylated at tyrosine-15, an ATP-binding site critical for the kinase function of CDC2 (Watanabe *et al.*, 1995), in untreated MOLM13 and MV4-11 cells. In contrast, CDC2-tyrosine 15 phosphorylation was not prominent in untreated THP-1 and U937 cells. These results suggest that CDC2 is relatively inactive in AML cell lines with FLT3 mutations, but is constitutively active in AML cell lines with wild-type FLT3. This pattern is fully compatible with the steady-state growth kinetics of these cells (Figure 1a). PKC412 modified the phosphorylation state of CDC2 in a reciprocal manner dependent on the presence of FLT3 mutations: CDC2 phosphorylation decreased

Table 1 Effects of PKC412 on cell cycle distribution of acute myeloblastic leukemia (AML) cell lines[a]

	MOLM13			*MV4-11*			*THP-1*			*U937*		
	Control	*PKC412*	P-*value**	*Control*	*PKC412*	P-*value**	*Control*	*PKC412*	P-*value**	*Control*	*PKC412*	P-*value**
12 h												
Sub-G_1	4.6±0.9	9.7±3.2	**0.04880**	5.6±0.8	6.8±1.7	0.21342	3.7±0.7	6.3±1.0	0.06957	3.7±0.8	3.3±0.8	0.21961
G_1	79.1±1.4	73.7±5.4	0.15931	82.6±3.2	81.2±1.8	0.36663	71.7±6.3	61.2±2.0	0.10660	79.3±2.2	22.1±3.4	**0.00022**
S+G_2/M	16.3±0.9	16.6±3.0	0.46585	11.8±2.5	12.0±2.7	0.47673	24.5±5.7	32.5±1.9	0.13740	17.1±2.6	74.6±4.2	**0.00023**
24 h												
Sub-G_1	7.8±0.7	14.4±2.9	**0.02911**	6.8±1.6	31.3±3.3	**0.00974**	2.6±0.7	3.8±0.7	0.13211	3.7±1.0	3.2±0.8	0.35510
G_1	72.0±1.8	79.2±2.8	**0.00553**	82.0±0.6	56.7±3.8	**0.00734**	67.8±2.0	27.6±3.2	**0.00406**	76.3±3.3	9.4±1.4	**0.00091**
S+G_2/M	20.2±1.3	6.4±0.8	**0.00384**	11.3±1.1	12.0±0.6	0.13694	29.6±2.5	68.5±3.7	**0.00632**	20.0±2.5	87.5±1.3	**0.00046**
48 h												
Sub-G_1	3.2±0.5	75.3±2.1	**0.00032**	4.4±1.4	59.2±3.5	**0.00196**	3.3±1.1	6.0±2.3	0.05624	4.6±0.7	5.7±1.5	0.09568
G_1	78.7±1.8	17.1±1.7	**0.00024**	84.1±3.6	34.3±1.9	**0.00299**	67.7±2.1	19.8±3.1	**0.00292**	76.3±3.2	8.8±2.5	**0.00046**
S+G_2/M	18.1±1.4	7.6±3.1	**0.00942**	11.5±2.6	6.5±1.7	**0.04318**	28.9±2.8	74.2±4.0	**0.00393**	19.0±4.0	85.5±3.5	**0.00033**

**P*-value was obtained by a paired Student's *t*-test between the data from untreated (control) and PKC412-treated (PKC412) cells ($n=3$). Data are the means±s.d. of three independent experiments. Bold values indicate $P<0.05$. [a]The proportion of cells in each phase of the cell cycle was calculated with the ModFitLT 2.0 program.

in MOLM13 and MV4-11, and increased in THP-1 and U937 after treatment with the drug. The inhibition of CDC2 kinase activity may underlie PKC412-induced G_2 arrest of THP-1 and U937 cells.

As Myt-1 kinase is responsible for CDC2 phosphorylation at tyrosine-15 (Galaktionov *et al.*, 1995), we examined the activation status of Myt-1 in these cells by immunoblotting with an antibody specifically recognizing the inactive/phosphorylated species of Myt-1. Consistent with the phosphorylation status of CDC2, Myt-1 was active (underphosphorylated) in AML cell lines with FLT3-ITD and inactive (phosphorylated) in AML cell lines without FLT3-ITD before treatment with PKC412 (Figure 3a). Myt-1 became phosphorylated and thereby inactivated by PKC412 in the former, whereas it became dephosphorylated and thereby activated in the latter, leading to the increased phosphorylation of CDC2. It is of note that Wee1, another kinase involved in tyrosine-15 phosphorylation, was below the detection limit in FLT3 mutation-positive leukemic cells as previously described (Neben *et al.*, 2005).

Next, we investigated the effects of PKC412 on the activity and intracellular localization of CDC25c, which activates CDC2 by removing phosphates from tyrosine-15. CDC25c was phosphorylated at serine-216 in untreated MOLM13 and MV4-11 cells, and was dephosphorylated by PKC412 (Figure 3a). In contrast, PKC412 increased the serine-216 phosphorylation of CDC25c in THP-1 and U937 cells. Upon phosphorylation at serine-216, CDC25c binds to 14-3-3 proteins and is translocated from the nucleus to the cytoplasm (Lopez-Girona *et al.*, 1999). We therefore confirmed the cytoplasmic sequestration of CDC25c phosphorylated at serine-216 using immunocytochemistry. As shown in Figure 3b, CDC25c was mostly retained in the cytoplasm in untreated MOLM13 cells, and was translocated to the nucleus after treatment with PKC412. In contrast, CDC25c was distributed throughout the entire cells in untreated U937 cells, and became sequestered in the cytoplasm and thus inactivated by the addition of PKC412. These observations are fully consistent with the pattern of serine-216 phosphorylation shown in Figure 3a. Furthermore, we demonstrated the binding of phosphorylated CDC25c to 14-3-3 proteins in cytoplasm using confocal microscopy. As shown in Figure 3c, phosphorylated CDC25c colocalized with 14-3-3 in untreated MV4-11 cells, and the interaction was dissociated after culture with PKC412. In U937 cells, PKC412 increased the amounts of phosphorylated CDC25c, which translocated from the nucleus and bound to 14-3-3 proteins in the cytoplasm. These results at least partly explain why PKC412 arrests cells in the G_2 phase of the cell cycle exclusively in AML cell lines without FLT3 mutations.

PKC412-induced apoptosis of AML cell lines with FTL3 mutations is mediated via selective phosphorylation of Bad at serine-128

Finally, we attempted to clarify the molecular mechanisms by which only AML cells with FLT3 mutations underwent apoptosis in the presence of PKC412. To this end, we screened for the expression of proapoptotic members of the Bcl-2 family by immunoblotting. As the expression of Bax and Bak was constitutive and unaffected by PKC412 in four AML cell lines (data not shown), we focused on BH3-only members of the Bcl-2 family, direct inducers of apoptosis (Galonek and Hardwick, 2006; Green, 2006). Among BH3-only proteins examined, only Bad was moderately expressed, and Bim, Bid, Puma and Noxa were undetectable in AML cell lines used in this study (data not shown). As PKC412 did not change the abundance of Bad protein, we examined the phosphorylation status of Bad using phosphorylation site-specific antibodies. It has been shown that Bad phosphorylation at various residues represents a checkpoint for the cell fate decision. For instance, CDC2 enhances the proapoptotic ability of

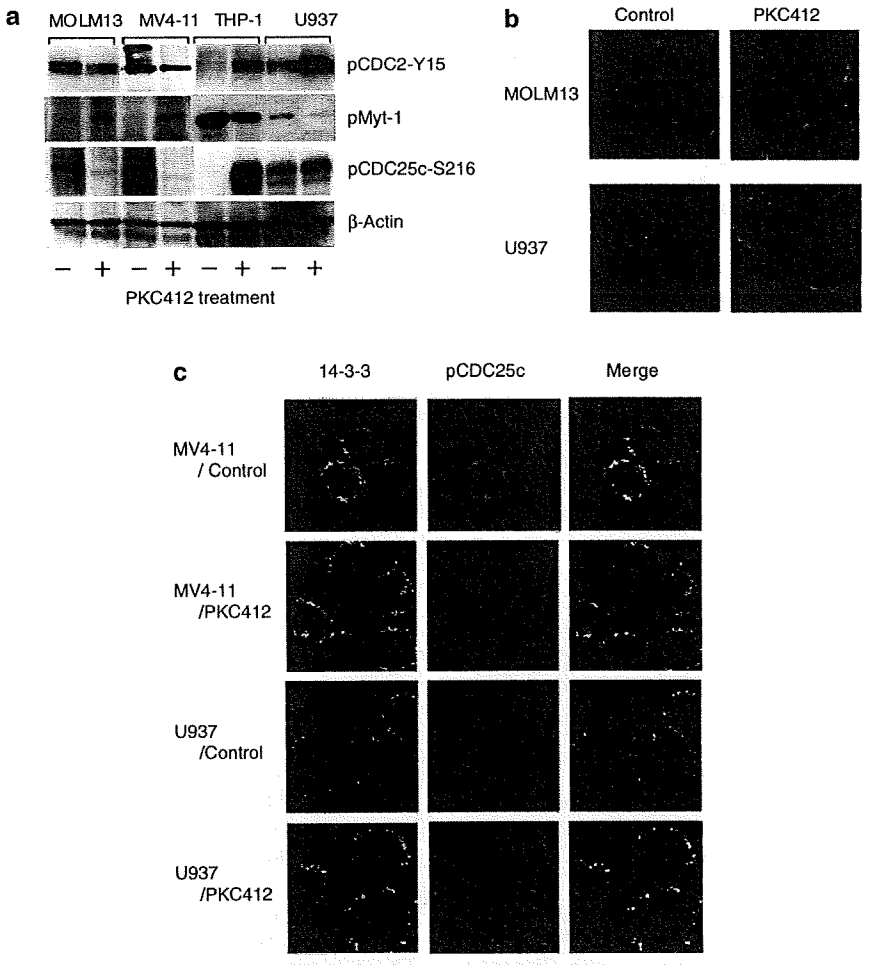

Figure 3 PKC412 differentially modulates CDC2 phosphorylation in acute myeloblastic leukemia (AML) cell lines depending on the presence of FLT3 mutations. (**a**) Whole cell lysates were prepared from AML cell lines before (−) and after (+) culture with 100 nM PKC412 for 24 h, and subjected to immunoblot analysis for the indicated proteins. (**b**) Intracellular localization of CDC25c was examined by immunocytochemistry in MOLM13 and U937 cells cultured in the absence (control) or presence (PKC412) of 100 nM PKC412 for 24 h. After being fixed, cells were stained with an anti-CDC25c monoclonal antibody and Alexa 488-conjugated goat antibody to mouse immunoglobulin. Original magnification is × 600 for all panels. (**c**) Colocalization of CDC25c and 14-3-3 proteins was examined by confocal microscopy in MV4-11 and U937 cells cultured in the absence (control) or presence (PKC412) of 100 nM PKC412 for 24 h. After being fixed, cells were stained with antibodies against 14-3-3 proteins and CDC25c phosphorylated at serine 216, followed by incubation with Alexa 488-conjugated goat antibody to mouse immunoglobulin and Cy3-conjugated goat antibody to rabbit immunoglobulin. Original magnification is × 600 for all panels. Data shown are representative of multiple independent experiments.

Bad by promoting serine-128 phosphorylation and mitochondrial translocation of Bad (Konishi *et al.*, 2002). In contrast, Akt promotes cell survival by phosphorylating Bad at serine-136, which provides a canonical binding site for 14-3-3 proteins to disrupt interaction with Bcl-2/Bcl-x on mitochondrial membranes (Zha *et al.*, 1996). Bad was phosphorylated at serine-136 and was inactive in untreated AML cells (Figure 4a, upper panel). Marginal levels of phosphorylation at serine-128 were observed in THP-1 and U937 cells, which may be due to the hyperactivation of CDC2. PKC412 induced Bad phosphorylation at serine-128 selectively in AML cell lines with FLT3-ITD along with dephosphorylation at serine-136 (Figure 4a, lower panel). AML cell lines with wild-type FLT3 did not show serine-128 phosphorylation. Next, we examined the intracellular localization of Bad using confocal microscopy. In untreated MV4-11 and U937 cells, Bad was distributed throughout the cytoplasm and did not colocalize with mitochondria (Figure 4b, Control). PKC412 induced the translocation of Bad to the mitochondria in MV4-11 cells but not in U937 cells (Figure 4b, PKC412). Intracellular localization of Bad is fully compatible with the alteration of site-specific phosphorylation of Bad, and at least partly explains the selective induction of apoptosis in AML cells with FLT3 mutations by PKC412.

Next, we determined the effects of PKC412 on the expression of antiapoptotic members of the Bcl-2 family. Immunoblot analyses revealed that AML cell lines used

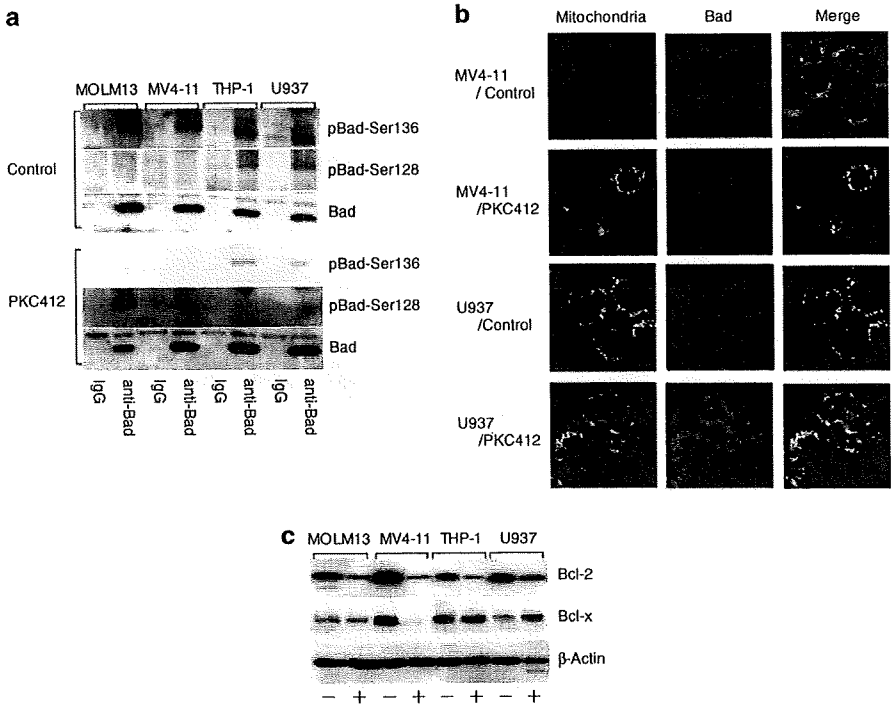

Figure 4 PKC412-induced apoptosis of acute myeloblastic leukemia (AML) cell lines with FTL3 mutations is mediated via phosphorylation of Bad at serine-128. (**a**) Whole cell lysates were prepared from AML cell lines cultured in the absence (control) or presence (PKC412) of 100 nM PKC412 for 24 h, and subjected to immunoprecipitation with either anti-Bad monoclonal antibody (anti-Bad) or mouse IgG (IgG). Immunoprecipitants were resolved on 12% acrylamide gels, followed by immunoblotting with polyclonal antibodies against Bad phosphorylated at serine-136, Bad phosphorylated at serine-128 and Bad. (**b**) For *in situ* visualization of Bad, we used anti-Bad polyclonal antibody and Cy3-conjugated goat antibody to rabbit immunoglobulin as primary and secondary antibodies, respectively. For co-labeling of mitochondria, we used a combination of anti-human mitochondria monoclonal antibody and Alexa 488-conjugated goat antibody to mouse immunoglobulin. (**c**) Protein samples in (**a**) were subjected to immunoblot analyses for Bcl-2, Bcl-x and β-actin (loading control). Data shown are representative of multiple independent experiments.

in this study expressed Bcl-2 and Bcl-x but not Mcl-1 and Bcl-w (data not shown). As shown in Figure 4c, Bcl-2 was readily downregulated by PKC412 in all four cell lines. The effects of PKC412 on Bcl-x expression were variable, suggesting that downregulation of Bcl-2 and Bcl-x is not a primary determinant of the sensitivity of AML cells to PKC412. However, it is possible that the reduced levels of Bcl-2 expression cooperate with the activation of Bad to enhance apoptosis in PKC412-treated MOLM13 and MV4-11 cells.

PKC412 induces apoptosis in primary AML cells with FTL3 mutations via the CDC2-Bad pathway

To testify the clinical relevance of our findings, we carried out the same experiments using primary AML cells from three patients with AML carrying FLT3-ITD. As shown in Figure 5a, PKC412 induced apoptosis with a decrease in the fraction of cells in the S phase in two cases and G_1 arrest with a moderate degree of apoptosis in one case. The effects of the drug on the phosphorylation status of FLT3, CDC2, Myt-1, CDC25c and Bad were almost identical to those observed in MOLM13 and MV4-11 cell lines (Figure 5b). There results indicate that our findings are not only valid in the cell line models, but have more general meanings.

Discussion

In this study, we obtained a clue pertinent to the molecular basis of the synergism and antagonism of PKC412 with other antileukemic agents. PKC412 alone induced G_2 arrest but not apoptosis in AML cell lines without aberrant FLT3 activation (THP-1 and U937) at a clinically achievable concentration. Because of the ability to cause G_2 arrest, PKC412 is synergistic with drugs that are active in the G_2/M phase, such as colchicine, in these cell lines. This may be an important advantage for the usage of PKC412 over other FLT3 inhibitors, because such effects have not been demonstrated with other FLT3 inhibitors (Levis *et al*., 2004; Yee *et al*., 2004). For the same reason, PKC412 may be antagonistic with drugs that synchronize target cells in late G_1 to early S phase, such as aphidicolin, in FLT3 mutation-negative leukemias. In contrast, PKC412-induced massive apoptosis without markedly affecting cell cycle patterns in AML cell lines harboring FLT3 mutations, which may underlie the synergism of PKC412 with most antileukemic agents.

Next, we attempted to elucidate the underlying mechanisms whereby PKC412 differentially affects the cell cycle distribution depending on the presence of FLT3 mutations. We obtained evidence suggesting that

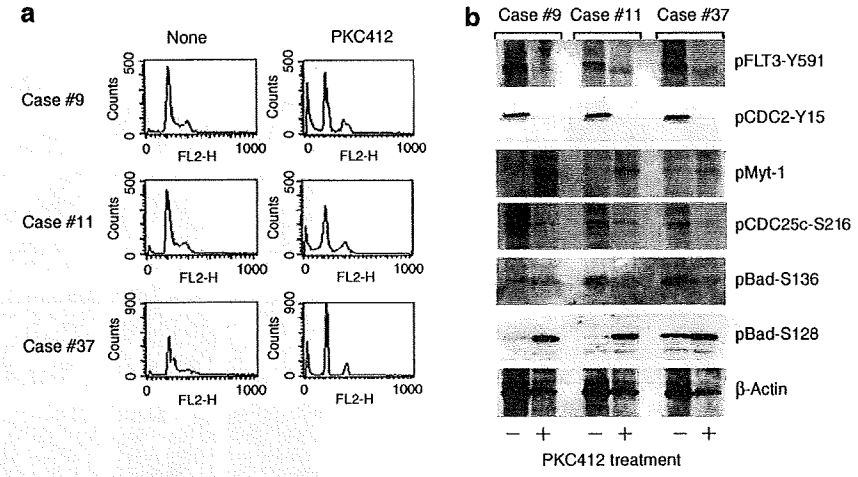

Figure 5 PKC412 induces apoptosis and cell cycle alterations in primary acute myeloblastic leukemia (AML) cells via the CDC2-Bad pathway. Bone marrow mononuclear cells from patients with AML carrying FLT3-ITD were cultured in the absence (none) or presence (PKC412) of 100 nM PKC412 for 24 h, and subjected to cell cycle analysis (**a**) and immunoblotting (**b**).

the cell cycle effect is mediated through the modulation of CDC2 activity by PKC412. The kinase activity of CDC2 is regulated by the opposing effects of specific kinases (Myt-1 and Wee1) and a specific phosphatase (CDC25c) on tyrosine-15, an ATP-binding site of CDC2 (Galaktionov *et al.*, 1995; Watanabe *et al.*, 1995). In untreated AML cell lines harboring FLT3-ITD, CDC2 was found to be at least partially inactivated by phosphorylation at tyrosine-15. This may be attributable to FLT3-ITD-mediated activation of Myt-1 kinase and inactivation of CDC25c by serine-216 phosphorylation and subsequent binding to 14-3-3 proteins. We are now trying to elucidate the signaling pathways of FLT3-ITD causing these changes. The partial inactivation of CDC2 may underlie the observation that AML cells with FLT3-ITD grow slower than those with wild-type FLT3. PKC412 reversed this process and activated CDC2 by promoting Myt-1 inactivation and facilitating nuclear translocation of CDC25c. In AML cells without FLT3-ITD, CDC2 is mostly in an active conformation and allows rapid cell cycling. PKC412 seems to inhibit CDC2 activity through CDC25c inactivation, which results in G_2 arrest. Although the precise mechanisms underlying this phenomenon are at present unknown, similar observations have been reported in non-small cell lung cancer and glioblastoma (Ikegami *et al.*, 1996; Begemann *et al.*, 1998).

Finally, we went on to identify target molecules responsible for selective induction of apoptosis in PKC412-treated AML cells with FLT3 mutations. To this end, we investigated the expression and function of Bcl-2 family proteins. Apoptotic cell death usually occurs through mitochondrial outer membrane permeabilization (MOMP), which is controlled by the balance between pro- and antiapoptotic members of the Bcl-2 family. Bad is a member of the BH3-only subfamily, and is known to promote MOMP by activating membrane-anchored proapoptotic Bcl-2 family proteins Bax and Bak (Galonek and Hardwick, 2006; Green, 2006). The function of Bad is tightly regulated by phosphorylation. For instance, the PI3 kinase-Akt pathway mediates phosphorylation of Bad at serine-136 and abrogates its proapoptotic activity (Zha *et al.*, 1996). It is well known that FLT3-ITD phosphorylates Bad through the Akt pathway and suppresses apoptosis of hematopoietic stem cells, which contribute to the development of leukemia (Kim *et al.*, 2006). In contrast, serine-128 phosphorylation promotes apoptosis in primary neurons by antagonizing survival functions of growth factors (Konishi *et al.*, 2002). Serine-128 phosphorylation is shown to be catalysed by CDC2 and c-Jun N-terminal kinase (Donovan *et al.*, 2002). Our results suggest that PKC412 causes phosphorylation of Bad at serine-128 via CDC2 activation along with dephosphorylation at serine-136 via blocking FLT3-ITD signaling, which results in apoptosis of AML cells with FLT3 mutations. In AML cells without FLT3-ITD, Bad phosphorylation at serine-128 did not occur because of PKC412-mediated inactivation of CDC2. Although serine-136 was dephosphorylated in some degree, these cells did not undergo apoptosis in response to PKC412. This is in line with a previous report that dephosphorylation of Bad is not sufficient and downregulation of Bcl-x is necessary for the induction of apoptosis (Yang *et al.*, 2005). In addition, Bcl-x inhibits CDC2 kinase activity at the G_2/M checkpoint by direct binding and causes G_2 arrest (Schmitt *et al.*, 2007). As Bcl-x was not downregulated in PKC412-treated THP-1 and U937 cells, it is possible that Bcl-x serves as an additional factor to determine the responses to PKC412.

Materials and methods

Reagents

PKC412 was purchased from LC Laboratories (Woburn, MA, USA), dissolved in dimethyl sulfoxide and stored at −20 °C until use.

Cells and cell culture
We used four human AML cell lines, that is, MOLM13, derived from a patient with acute monocytic leukemia (AMoL) carrying t(9;11); MV4-11, derived from a patient with AMoL carrying t(4;11); THP-1 and U937, derived from patients with AMoL without FLT3 mutations. MV4-11, THP-1 and U937 were purchased from the American Type Culture Collection (Manassas, VA, USA), and MOLM13 was provided by Dr Yoshinobu Matsuo (Grandsoul Research Institute for Immunology, Nara, Japan). These cell lines were maintained in RPMI1640 medium supplemented with 10% fetal bovine serum. Primary AML cells were isolated from the bone marrow of patients at the time of diagnostic procedure. Informed consent was obtained in accordance with the Declaration of Helsinki, and the protocol was approved by the institutional review board. The presence of FLT3-ITD was examined as described by Kiyoi *et al.* (1997).

Flow cytometric analysis
The cell cycle profile was obtained by staining DNA with Vindelov's solution (0.04 mg ml^{-1} propidium iodide in 5 mM Tris–HCl, 5 mM NaCl and 0.005% nonidet P-40) in preparation for flow cytometry. The size of the sub-G_1, G_0/G_1 and $S+G_2/M$ fractions was calculated as a percentage by analysing DNA histograms with the ModFitLT 2.0 program (Verity Software, Topsham, ME, USA). Surface marker analysis was carried out according to the standard method.

Immunocytochemistry
After collecting on glass slides using a Cytospin centrifugator (Shandon Scientific, Cheshire, England), cells were fixed in 4% paraformaldehyde in phosphate-buffered saline, and stained with a rabbit antitubulin polyclonal antibody (Sigma, St Louis, MO, USA) and Alexa 488-conjugated goat antibody to rabbit immunoglobulin (Molecular Probes, Eugene, OR, USA) as primary and secondary antibodies, respectively. Finally, nuclear DNA was stained with 100 ng ml^{-1} propidium iodide in phosphate-buffered saline for 5 min.

Detection of apoptosis
Apoptosis was detected *in situ* by the TUNEL (TdT-mediated dUTP-biotin nick end labeling) method using MEBSTAIN apoptosis kit (MBL International, Woburn, MA, USA). In brief, cells were fixed on glass slides as described above, and treated with terminal deoxynucleotidyl transferase (TdT) in the presence of biotin-dUTP to label 3′-ends of fragmented DNA. The labeled ends were visualized with avidin-conjugated fluorescein isothiocyanate (FITC). Finally, intact DNA was counterstained with propidium iodide.

Confocal laser microscopy
Confocal microscopic analysis was performed using the following antibodies: anti-CDC25c (C2-2; BD Pharmingen, San Jose, CA, USA), antiphosphorylated CDC25c at serine-216 (no. 4901; Cell Signalling Technology, Beverly, MA, USA), anti-human 14-3-3 (C23-1; BD Pharmingen), anti-Bad (no. 9292; Cell Signalling Technology) and anti-human mitochondria (AE-1; Leinco Technologies Inc., St Louis, MO, USA). We used Alexa 488-conjugated goat antibody to mouse immunoglobulin (Molecular Probes) and Cy3-conjugated goat antibody to rabbit immunoglobulin (Amersham Pharmacia Biotech, Piscataway, NJ, USA) as secondary antibodies.

Immunoprecipitation and immunoblotting
Immunoprecipitation and immunoblotting were carried out according to the standard methods using the following antibodies: anti-FLT3 (8F2; Santa Cruz Biotechnology, Santa Cruz, CA, USA), antiphosphorylated FLT3 at tyrosine-591 (no. 3461; Cell Signalling Technology), antiphosphorylated protein kinase C (pan) at serine-660 (no. 9371; Cell Signalling Technology), antiphosphorylated c-Kit at tyrosine-719 (no. 3391; Cell Signalling Technology), antiphosphorylated PDGF receptor β at tyrosine-751 (no. 3161; Cell Signalling Technology), antiphosphorylated CDC2 at tyrosine-15 (no. 9111; Cell Signalling Technology), anti-Bad monoclonal (clone 48; BD Transduction Laboratories, San Jose, CA, USA), anti-Bad polyclonal (no. 9292; Cell Signalling Technology), antiphosphorylated Bad at serine-136 (no. 9295; Cell Signalling Technology), antiphosphorylated Bad at serine-128 (AB3567; Chemicon International, Temecula, CA, USA), anti-Bcl-2 (clone 4D7; BD Transduction Laboratories), anti-Bcl-x (clone 44; BD Transduction Laboratories) and anti-β-actin (C4; ICN Biomedicals, Aurora, OH, USA).

Acknowledgements

This work was supported in part by the High-Tech Research Center Project for Private Universities: Matching Fund Subsidy from MEXT 2002–2006, and grants from the Vehicle Racing Commemorative Foundation and Sankyo Foundation of Life Science (to YF). JK is a winner of the Jichi Medical School Young Investigator Award. TW is a winner of the Jichi Medical School Graduate Student Award.

References

Begemann M, Kashimawo SA, Heitjan DF, Schiff PB, Bruce JN, Weinstein IB. (1998). Treatment of human glioblastoma cells with the staurosporine derivative CGP 41251 inhibits CDC2 and CDK2 kinase activity and increases radiation sensitivity. *Anticancer Res* **18**: 2275–2282.

Donovan N, Becker EB, Konishi Y, Bonni A. (2002). JNK phosphorylation and activation of BAD couples the stress-activated signaling pathway to the cell death machinery. *J Biol Chem* **277**: 40944–40949.

Furukawa Y, Vu HA, Akutsu M, Odgerel T, Izumi T, Tsunoda S *et al.* (2007). Divergent cytotoxic effects of PKC412 in combination with conventional antileukemic agents in FLT3 mutation-positive versus negative leukemia cell lines. *Leukemia* **21**: 1005–1014.

Galaktionov K, Jessus C, Beach D. (1995). Raf1 interaction with Cdc25 phosphatase ties mitogenic signal transduction to cell cycle activation. *Genes Dev* **9**: 1046–1058.

Galonek HL, Hardwick JM. (2006). Upgrading the bcl-2 network. *Nat Cell Biol* **12**: 1317–1319.

Gilliland DG, Griffin JD. (2002). The roles of FLT3 in hematopoiesis and leukemia. *Blood* **100**: 1532–1542.

Green DR. (2006). At the gates of death. *Cancer Cell* **9**: 328–330.

Griffin JD. (2004). FLT3 tyrosine kinase as a target in acute leukemias. *Hematol J* **5**: 188–190.

Ikegami Y, Yano S, Nakao K. (1996). Effects of the new selective protein kinase C inhibitor 4′-N-benzoyl staurosporine on cell cycle distribution and growth inhibition in human small cell lung cancer cells. *Arzneimittelforschung* **46**: 201–204.

Kelly LM, Liu Q, Kutok JL, Williams IR, Boulton CL, Gilliland DG. (2002). FLT3 internal tandem duplication mutations associated with human acute myeloid leukemias induce myeloproliferative disease in a murine bone marrow transplant model. *Blood* **99**: 310–318.